TECHNICAL UNIVERSITY – SOFIA
English Language Faculty of Engineering

RESEARCH PROJECT

MEng Degree

"Modelling, Analysis and Options for Improvement of Horizontal Axis Wind Turbine Design"

Name: Cristina Rebollo Mugueta

Supervisor: Assoc. Prof. Yanko Slavchev

Sofia 2014

TECHNICAL UNIVERSITY - SOFIA

ENGLISH LANGUAGE FACULTY OF ENGINEERING

Deadline:

Dean: ……
Name: **Prof. PhD T. Tashev**

FINAL YEAR PROJECT ASSIGNMENT
MEng course

1. Student's name: **Cristina Rebollo Mugueta**

2. Project title: **Modelling, Analysis and Options for Improvement of Horizontal Axis Wind Turbine Design**

3. Basic project specifications:
   A downwind horizontal axis wind turbine (HAWT); steel monopole tower, 72 meters high; 3-bladed wind turbine rotor; blade airfoil NACA0021; blade span 30 meters; tower and blades - systems with distributed parameters; nacelle - concentrated mass; wind speed variation according to Log-wind profile.

4. Contents:
   a) Introduction
   b) Types of wind turbines
   c) Wind models
   d) Aerodynamic concepts
   e) Wind power extraction
   f) Modelling, simulations and analyses
   g) Conclusions

Project supervisor: ……
Name: **Assoc. Prof. PhD Y. Slavchev**

Deputy Dean: ……
Name: **Assoc. Prof. PhD R. Dinov**

CONTENTS

LIST OF SYMBOLS

a' pre-rotational factor (disk rotor theory)

A- Planform area

B Number of blades on turbine

c Chord length [m]

$\mathbf{C_D}$ Coefficient of drag

$\mathbf{C_L}$ Coefficient of lift

Cp Coefficient of power

$\mathbf{C_T}$, $\mathbf{C_B}$ Damping in the tower and blade

D drag [N]

$\mathbf{D_{T1}}$, $\mathbf{D_{T2}}$ Outer diameters at the tower tip and foundation

$\mathbf{D_{B1}}$, $\mathbf{D_{B2}}$ Chords at the base and blade tip

$\mathbf{E_T}$, $\mathbf{E_B}$ Elasticity moduli of the tower and the blade

$\mathbf{f_B}$, $\mathbf{f_T}$ Distributed load along the blade and tower

F Concentrated load on the Nacelle

l Length

$\mathbf{L_T}$, $\mathbf{L_B}$ Length of the tower and blade

$\mathbf{J_T}$, $\mathbf{J_B}$ Moments of inertia

L lift [N]

L/D Lift-to-drag ratio

m mass [kg]

$\mathbf{m_T}$, $\mathbf{m_B}$ Distributed mass of the tower and blade

M Mach number

p pressure [Pa]

$\mathbf{P_{rotor}}$ Power in the rotor

$\mathbf{P_a}$ Available power

P_c Captured power

r local radius from the root blade [m]

R full radius [m]

Re Reynolds number

t time

T Tower

u Flow speed in boundary layer [m/s]

U Local or Axial wind speed [m/s]

V Relative or Tangential wind speed [m/s]

W Apparent wind speed [m/s]

w Displacement

x Height

λ tip speed ratio

φ flow angle inclination [deg]

α angle of attack [deg]

α' Hellman exponent

α_t Tilt angle

α_c Cone angle

β pitch angle [deg]

Ω Rotational speed [s-1]

η mechanical efficiency

ρ density [kg/m3]

μ dynamic viscosity [kg/(m ^{2}s)]

υ kinematic viscosity [m ^{2}/s]

ACKNOWLEDGEMENTS

This thesis work has been conducted at Technical University of Sofia, English Language Faculty of Engineering.

It's a great pleasure to thank everyone who helped me accomplish the thesis. I am truly indebted and thankful to my supervisor, Professor Yanko Slavchev, whose help, stimulating suggestions and encouragement was a great source of energy in all the time of my research.

Besides, I would like to thank my coordinator, Professor Vladislav Slavov and the Dean English language faculty of engineering dean, Tasho Tashev, for helping me with the paperwork from day to day to make this work in a country that is so far away from mine. During last months, they have shown me their concern about how my work is going and they helped me to choose the most appropriate area for my master thesis in addition to putting me in touch with the most suitable Professor.

Last but not the least, my deepest gratitude goes to my family and friends, for their support through my life.

1. AIM OF THE THESIS

Eolic technology is considered one of the most promising areas of renewable energy sources. However, the manufacturing and installation of wind turbines are quite costly and produce pollutants. Furthermore, wind turbines are subject to different and sometimes unknown types of aerodynamic loadings in their life time operation.

The objective of this paper is to model, simulate and analyse the response of a computer modelled HAWT and eventually propose and study options for its improvement, primarily through the introduction of modern blade airfoils. The modelling and simulation (M&S) stage encompasses the use of computer-aided design (CAD) applications for constructing the model as well as computational tools like the finite element method (FEM), the blade element method (BEM), the Newmark method, computational fluid dynamics (CFD) and others for simulating and analysing the response of the HAWT both in its default design configuration and in the improved design configuration.

The computational tools are properly combined so that on one hand to be able to compare the results for the proposed cases and on the other hand to be more computationally effective. The effectiveness pursuit is both in time and in the available hardware resources.

2. INTRODUCTION

The energy crisis in the world is going to be, in the next 100 years when the Earth's supply of fossil is no more, isn't foreign matter to anyone. Since the start of the industrial revolution humans have been using fossil fuels to power their machines that make more machines. Society thinks that the "gravy train" that is fossil fuels will be around for a long time but analysis on the current supplies and the ever growing population of the planet suggest that we may run out very soon. The Klass model assumes a continuous compound rate and it is a computational approximation of when we will run out of the various fossil fuels. Depletion times for oil, coal and natural gas are approximately 35, 107, and 37 years. These figures do not give much time for alternative methods to be found or perfected.

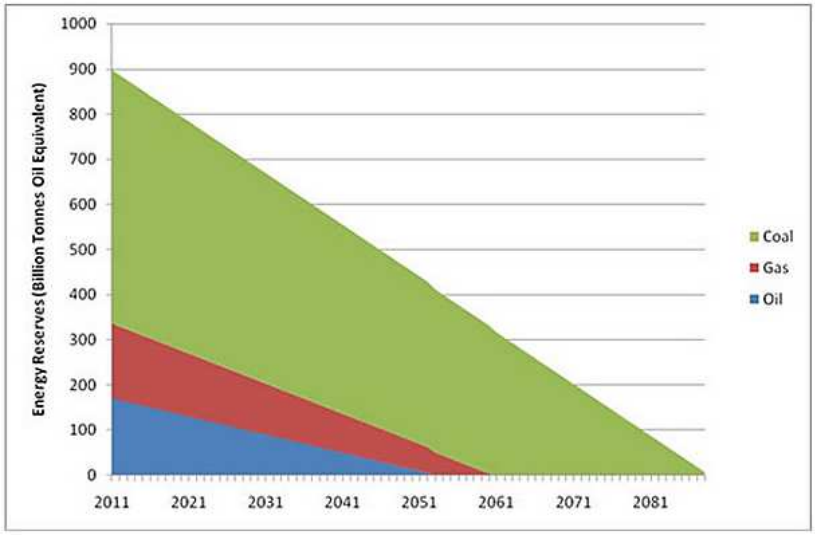

Figure 1. Energy reserves.

It's often claimed that we have enough coal to last hundreds of years. But if we step up production to fill the gap left through depleting our oil and gas reserves, the coal deposits we know about will only give us enough energy to take us as far as 2088. And let's not even think of the carbon dioxide emissions from burning all that coal.

The actual society absolutely depends of energy production but day by day there is more energy demands and energetic resources like fossil fuels are daily lower. Hence, in the actual situation, is necessary to investigate on energy sources that don't use fossil fuels.

In the following figure, can be noticed the world´s energetic demands and estimation during next 25 years.

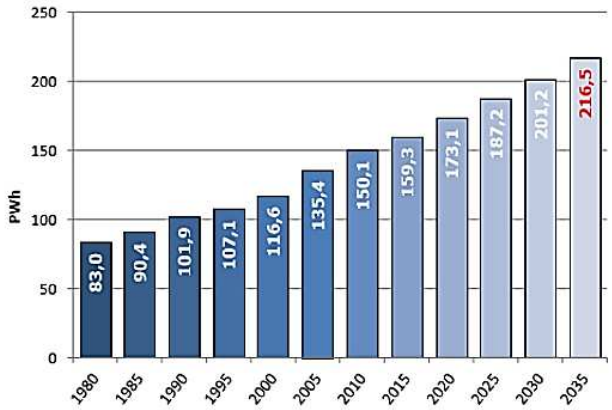

Figure 2.World's energetic demands evolution (EIA 2010)

According to Pike Research´s (market research and consulting firm) report [2], the largest markets for offshore wind through the remainder of this decade will be in Western Europe, which as a region will account for fully 75% of global installed capacity in 2017.

However, this forecast was developed before the news about Greece, the potential for more bank bailouts, and the ongoing fears of a double-dip recession across the globe. Therefore, its momentum on the clean energy front in the face of steep cuts in subsidies for Feed-in-Tariffs (FITs) that have been responsible for almost half of the world´s current renewable energy generation.

However, the current financial crisis may actually sustain investments in renewables in Europe. Don't forget, unlike the U.S., Europe actually has a mandate to cut carbon emissions.

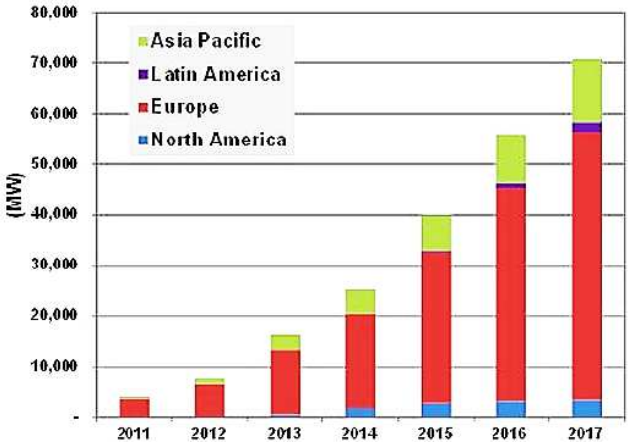

Figure 3. Offshore wind capacity installed.

Among renewables, installed hydroelectric power capacity is expected to increase more than other renewable sources between 2008 and 2035. However, installed solar power capacity sees the largest growth rate over the projection period, expanding 8.3% per

year, followed by 5,7% for wind, 3.7% for geothermal, 2.0% for hydropower, and 1.4% for other renewables such as wood waste, landfill gas, and agricultural by products.

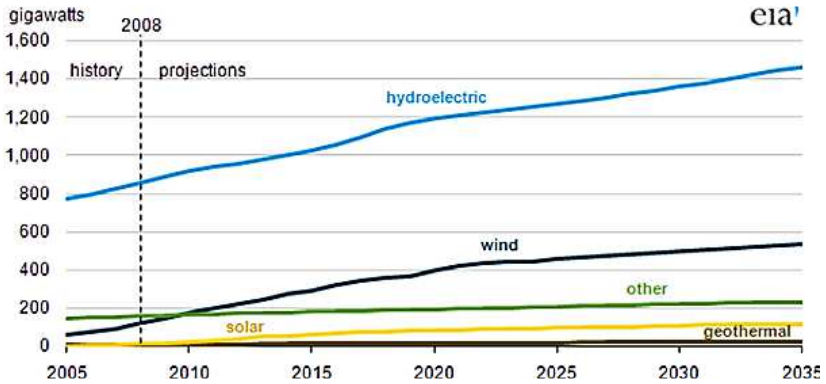

Figure 4. Global installed power generation capacity by renewable source.

Hence, wind power is a strong candidate towards a sustainable future; wind power with hydro power are among the most effective renewable energies. For many countries, with its relatively fast development potential, wind power presents a good starting point for developing renewable energy sources. However, due to its variability, it cannot aim to be the only electricity source for a single country.

Therefore, the use of wind turbines on residential and commercial properties could help to extend the energy reserves deadlines out further or even eliminate them if the right technologies come about.

3. TYPES OF WIND TURBINES

Although there are many different wind turbine designs, they are broadly grouped in two categories based on the orientation of the axis of rotation: Horizontal Axis Wind Turbines, or HAWTS, the most common type of wind turbine, and Vertical Axis Wind Turbines, or VAWTS.

3.1. VAWTS

There are two main types of VAWTs, the Savonius and the Darrieus. The Savonius operates like a water wheel using drag forces, while the Darrieus uses blades similar to those used on HAWTS. VAWTs typically operate closer to the ground, which has the advantage of allowing placement of heavy equipment, like the generator and gearbox, near ground level rather than in the nacelle. However, winds are lower near ground level, so for the same wind and capture area, less power will be produced.

Another advantage of a VAWT over the HAWT is that it doesn't require a yaw mechanism, since it can harness wind from any direction. This advantage is outweighed by many other disadvantages, including: time varying power output due to variation of power during a single rotation of the blade, the need for guy wires to support the tower and the fact that Darrieus VAWTS are not self starting like HAWTS.

Figure 5. Darrieus wind turbines examples.

Figure 6. Savonius wind turbines examples

3.2. HAWTS

Its main feature is that the axis rotation is parallel to the ground and the wind direction. Modern HAWTs usually feature rotors that resemble aircraft propellers, which operate on similar aerodynamic principles, i.e., the air flow over the airfoil shaped blades creates a lifting force that turns the rotor.

Among its advantages HAWTS can be placed on towers to take advantage of higher winds farther from the ground. The nacelle of a HAWT houses a gearbox and generator. However, this capture area must face directly into the wind, to maximize power generation, so HAWTS require a means for alignment (yawing mechanism) so that the entire nacelle can rotate into the wind. On smaller wind turbines, a tail vane provides a "passive" yaw control. In large, grid-connected turbines, yaw control is active, with wind direction sensors and motors that rotate the nacelle.

Figure 7. HAWT offshore example.

3.2.1. Number of blades

The determination of the number of blades involves design considerations of aerodynamic efficiency, component costs, and system reliability. Depending on the number of blades, the turbines can be divided into one bladed, two bladed, three-blade and multi-blade.

The one bladed, are formed by a single blade and require a counterweight at the other end to balance. Allow for higher speed, reduced masses and costs of materials, blades and the gearbox. They have the disadvantage of requiring a very accurate balanced with a counterweight offset, and there is increased risk of aerodynamic imbalance and vibration with the appearance of fatigue loads.

Figure 8. One bladed wind turbine.

Two bladed wind turbines have the advantage of saving the cost of a blade, compared to the three-bladed and of course, weight. However, they often have difficulty entering the market, partly because they need a higher rotational speed to produce the same energy output. This is a disadvantage both in relation to noise and visual appearance.

Figure 9. Two bladed wind turbine.

The three-bladed wind turbines are wind turbines quintessential today; most of the designs are placed with three blades 120 degrees between them. Its main advantage is that give the structure a more balanced designs than one or two blades and obtain better performance. A greater number of blades increase the weight and cost of the wind turbine, so this type of turbine is not used for power generation but for pumping water.

Figure 10. Three bladed wind turbine.

Figure 11. Multibladed wind turbine.

Noise emissions are affected by the location of the blades upwind or downwind of the tower and the speed of the rotor.

3.2.2. Rotor position

Some wind turbines are designed to operate in an upwind mode, the shaft of the rotor and generator are positioned horizontally and the wind hits blade before the tower. Large wind turbines use a motor-driven mechanism that turns the machine in response to a wind direction. Smaller wind turbines use a tail vane to keep the blades facing into the wind.

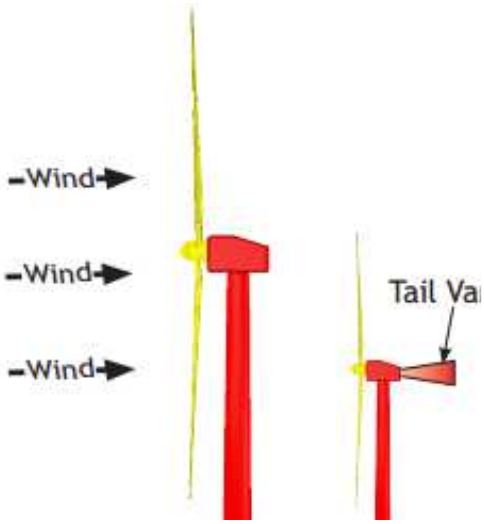

Figure 12. Upwind turbine.

Its advantage is the reduced tower shading. The air will start to bend around the tower before it passes it so there is some loss of power from the interference, just not the degree as in the downwind turbine.

However, its disadvantage is the extended nacelle that is required to position the rotor far enough away from the tower to avoid any problems with a blade strike. The

blades themselves must be somewhat stiff to avoid bending back into the tower. This will mean the point where the blade attaches to the rotor hub will be stressed during high, gusty wind conditions.

Other wind turbines operate in a downwind mode so that the wind passes the power before striking the blades. Without a tail vane, the machine rotor naturally tracks the wind in a downwind mode.

Their advantages are that the rotor blades can be flexible since there is no danger of a tower strike. Thus, they can be less expensive to make and they can relieve stress on the tower during high or gusty wind conditions since the flexing allows some wind load to be transferred directly to the blades instead of the tower.

The flexible blade advantage can also be a disadvantage as the flexing may fatigue the blades. Tower shadow is problem with a downwind machine since the rotor blade actually passed behind the tower. This can cause turbulence and increased fatigue on the unit.

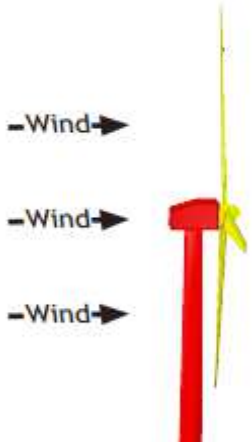

Figure 13. Downwind turbine.

3.2.3. Tilt angle/Cone angle

The angle between the horizontal axis and the rotor shaft is defined as tilt angle (α_t). A positive angle increases hub height and tower clearance. Axis tilt is kept to a minimum because of potential negative effects, such as reduced swept area and a vertical component to the rotor torque that can cause a yaw moment on the nacelle.

On the other hand, the angle between the rotor plane and the blade axis is defined as cone angle (α_c). The cone angle improves stability around the axis of yaw in the wind rotor.

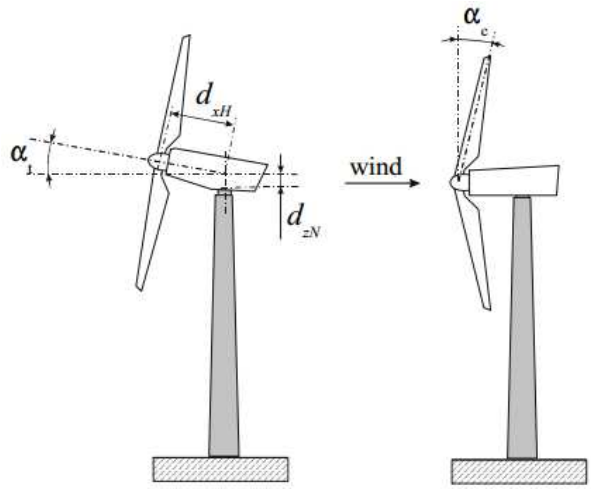

Figure 14. Tilt angle and cone angle in an upwind turbine.

3.2.4. Power control types

All wind turbines are designed with some sort of power control. There are different ways to control aerodynamic forces on the turbine rotor, and thus to limit the power in very high winds in order to avoid damage to the wind turbine:

- **Stall control (passive control)**: It is the simplest, most robust and cheapest control method, where the blades are bolted onto the hub at a fixed angle. The design of rotor aerodynamics causes the rotor to stall (lose power) when the wind speed exceeds a certain level. Thus, the aerodynamic power on the blades is limited. Such slow aerodynamic power regulation causes less power fluctuation than a fast-pitch power regulation. Some drawbacks of the method are lower efficiency at low wind speeds, no assisted start up and variations in the maximum steady-state power due to variations in air density and grid frequencies.

- **Pitch control (active control)**: The blades can be turned out or into the wind as the power output becomes too high or too low respectively. Generally, the advantages of this type of control are good power control, assisted start up and

an emergency stop. Some disadvantages are the extra complexity arising from the pitch mechanism.

- **Active stall control**: The stall of the blade is actively controlled by pitching the blades. At low wind speeds the blades are pitched similar to a pitch-controlled wind turbine, in order to achieve maximum efficiency. At high wind speeds the blades go into a deeper stall by being pitched slightly into the opposite direction from that of a pitch-controlled turbine. The active stall wind turbine achieves a smoother limited power, without the high power fluctuations as in the case of pitch-controlled wind turbines. This control type has the advantage of being able to compensate variations in air density. The combination with the pitch mechanism makes it easier to carry out emergency stops and to start up the wind turbine.

4. WIND MODEL

Wind turbines interact with the wind, capturing part of its kinetic energy and converting it into usable energy. This energy conversion is the result of several phenomena. The wind is characterized by its speed and direction, which are affected by several factors, e.g. geographic location, climate characteristics, height above ground, and surface topography.

4.1. WIND VARIATION IN SPACE

The wind in a given site near the surface of the Earth results from the combination of the geostrophic and local winds. Therefore, it depends on the geographic location, the climate, the height above ground level, the roughness of the terrain and the obstacles in the surroundings. These are the winds the wind turbines interact with. An interesting characterization of these surface winds is their kinetic energy distribution in the frequency domain.

4.1.1. Macro-scale

In a macro-meteorological sense, winds are movements of air masses in the atmosphere mainly originated by temperature differences. The temperature gradients are due to uneven solar heating. In fact, the equatorial region is more irradiated than the polar ones. Consequently, the warmer and lighter air of the equatorial region rises to the outer layers of the atmosphere and moves towards the poles, being replaced at the lower layers by a return f ow of cooler air coming from the Polar Regions. This air circulation is also affected by the Coriolis forces associated with the rotation of the Earth. In fact, these forces def ect the upper f ow towards the east and the lower f ow towards the west. These large-scale air f ows that take place in the entire atmosphere constitute the geostrophic winds.

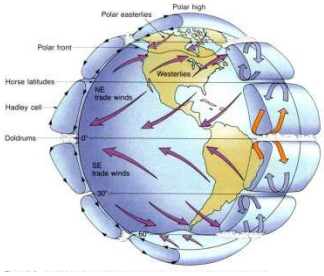

Figure 15. Idealized global wind´s circulation.

4.1.2. Meso-scale

Meso scale wind systems are also known as storm scale weather systems. Included in this meteorological scale are thunderstorms, squall lines, meso-scale convective systems (MCS), frontal boundaries, land and sea breezes, and mountain and valley breezes. Meso-scale systems range from 50 miles to several hundred miles in length.

In coastal regions, sea breezes and land breezes can be important factors in a location's prevailing winds. During the day, the temperature of the surface of the land rises, the land heats the air above it by conduction. The warm air is less dense than the surrounding environment and so it rises. The cooler air above the sea, now with higher sea level pressure, flows inland into the lower pressure, creating a cooler breeze near the coast. This phenomenon is opposite during the night.

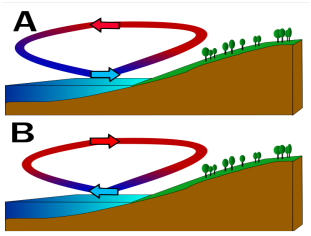

Figure 16. A) sea breeze during the day, B) sea breeze during the night.

Foehn winds are caused by the subsidence of moist air after passing a high mountain. The air is forced to move upslope when encounters a mountain barrier. As the temperature decreases with height, the moist air will become saturated and condense to form clouds and rain when it rises to a certain height. The amount of water vapour that

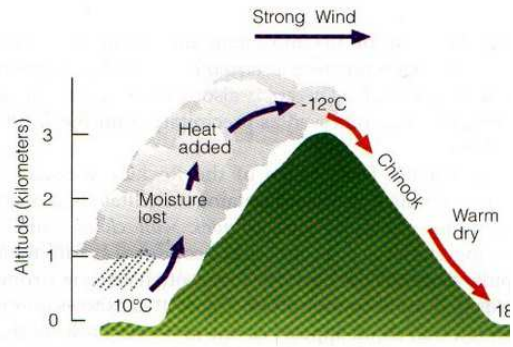

Figure 17. Foehn effect.

remains in the air therefore decreases. After passing the ridge and descending along the leeside of the mountain, the air becomes warmer. Temperature of drier air will rise even faster. This results in dry and hot winds.

4.1.3. Micro-scale

The lower layer of the atmosphere is known as surface layer and extends to a height of 100 m. In this layer, winds are delayed by frictional forces and obstacles altering not only their speed but also their direction. This is the origin of turbulent f ows, which cause wind speed variations over a wide range of amplitudes and frequencies.

In complex terrains, the medium wind speed is higher than in flat areas and the velocity distribution is also more irregular. Turbulence is quantified with a metric called turbulence intensity. Atmospheric turbulence impacts wind energy in several ways, specifically through power performance effects, impacts on turbine loads, fatigue and wake effects, and noise propagation.

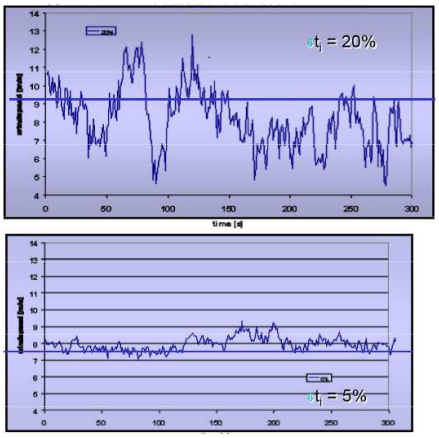

Figure 18. Turbulence comparison between complex and plain terrain.

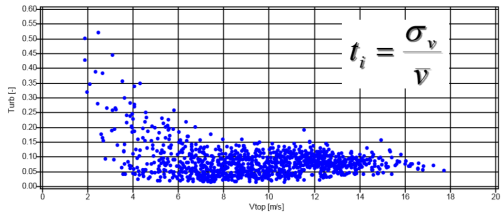

Figure 19. Turbulence intensity distribution.

The effects of **wind shear** are also of certain importance in better understanding wind behaviour. The idea of wind shear is the change in wind directions at different elevations. The factors that influence in wind profile are terrain roughness, the atmospheric stability and the orography.

For wind turbine engineering, an exponential variation in wind speed with height can be defined relative to wind measured at a reference height of the low blade as:

$$v_{top} = v_{LowBlade}\left(\frac{h_{top}}{h_{LowBlade}}\right)^{\alpha'} \qquad \text{[Equation 1]}$$

The Hellman exponent (α') depends upon the coastal location and the shape of the terrain on the ground, and the stability of the air. Examples of values of the Hellman exponent are given in the table below:

Table 1. Variation of the Hellman exponent depending on the location.

location	α
Unstable air above open water surface:	0.06
Neutral air above open water surface:	0.10
Unstable air above flat open coast:	0.11
Neutral air above flat open coast:	0.16
Stable air above open water surface:	0.27
Unstable air above human inhabited areas:	0.27
Neutral air above human inhabited areas:	0.34
Stable air above flat open coast:	0.40
Stable air above human inhabited areas:	0.60

In this case, the above equation shows an exponential variation in wind speed with height relative to wind measured at a reference height of the low blade. However, the wind speed variation according to the height can be seen in the figure below and later in equation [23].

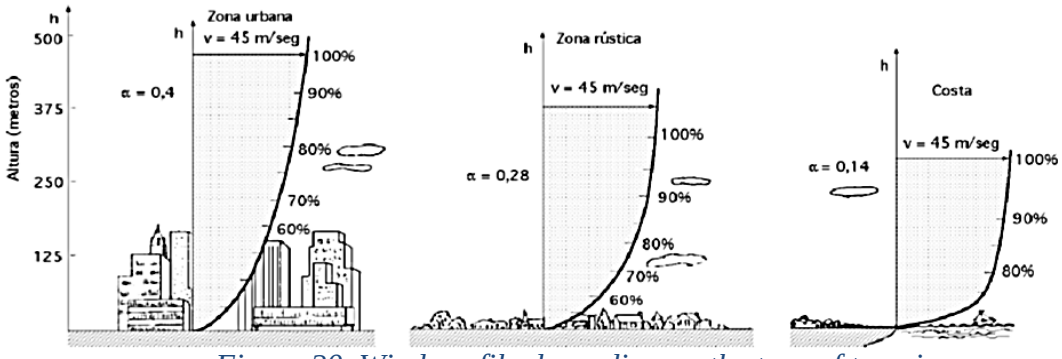

Figure 20. Wind profile depending on the type of terrain.

Moreover, atmospheric stability influence wind speed profile like is shown in the figure below:

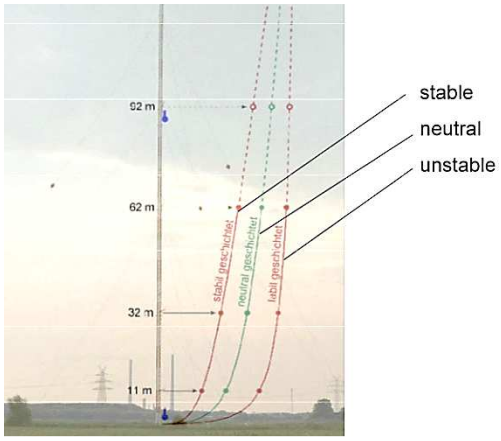

Figure 21. Influence of atmospheric stability in wind speed profile.

The influence of day (unstable) and night (stable) is shown in the following figure. Average wind speed increase between 50 and 100 m during the measurement period is 9% during the day (unstable stratification) and 16% during the night (stable stratification).

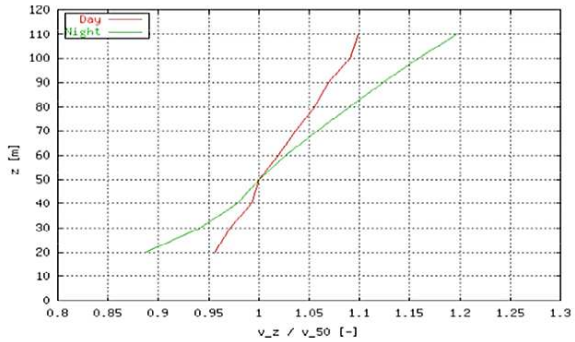

Figure 22. Influence of day and night in wind speed profile for one direction and complex terrain.

4.2. WIND VARIATION ON TIME

The wind is constantly changing in speed and in direction also. The wind speed varies during the year because of seasonal changes and hence temperature. In addition, also varies along the day, as can be seen in the following figure it is lower during the night due to atmospheric stability.

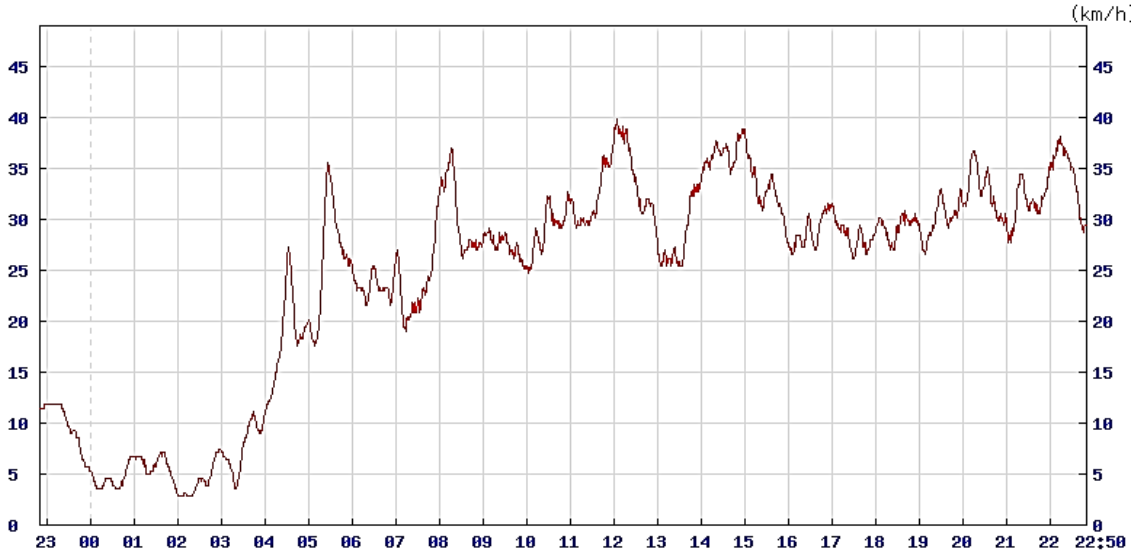

Figure 23. Variation of wind speed during a day in Cheung Chau Island (Hong Kong).

In addition, the wind direction can change and a correct orientation of the HAWT allows better energetic utilization of the site and avoid others wind turbine´s wakes. A wind rose is a graphic tool used to give a succinct view of how wind speed and direction are typically distributed at a particular location. For example, the wind rose below indicates that most of time the wind blows from the west and south-west and that these winds are also the strongest and therefore potentially those which will generate the most energy.

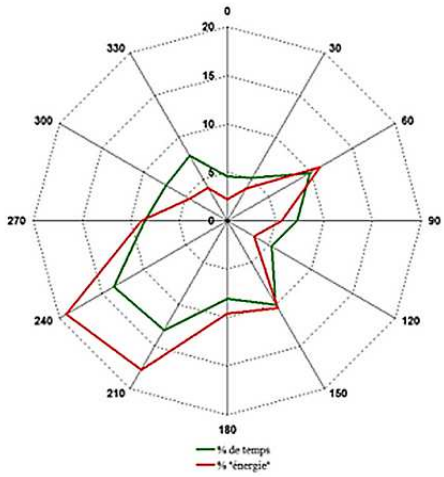

Figure 24. Wind rose example that represent direction and wind power.

Variability is a major problem associated with wind power. If the wind is too weak, very little power is generated. But, if it's too strong, the large forces exerted may cause structural damage, so many turbines shut down in high winds. The variations in wind speed are often modelled statistically using a Weibull curve (see Figure 25). In essence, for a

given annual average wind speed, the Weibull curve provides an estimate of how many hours per year the wind will be within a range of values.

In addition to day-to-day variability, winds are rarely steady. Instead, they are almost always gusting. This turbulence leads to two problems:

- The electrical power output of the generator will constantly vary, requiring proper conditioning.
- The continually changing forces on the blades results in fatigue loading that is the main factor in how long a blade can be run before needing replacement.

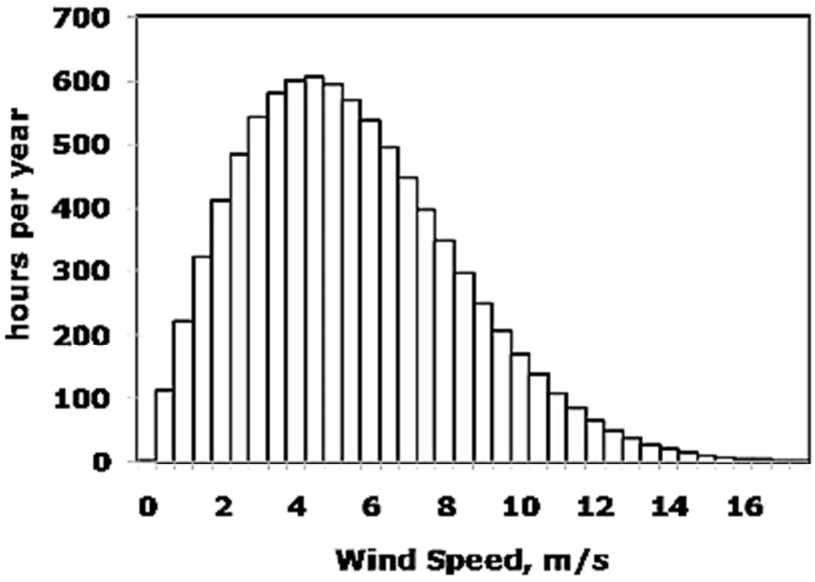

Figure 25. Annual wind speed distribution.

This plot shows the expected hours per year that the wind speed will be at a certain value (±0.25m/s), for the site with a mean annual wind speed of 5.5 m/s. For example, the winds speed will be between 3.75m/s and 4.25 m/s for 600 hours per year.

5. AERODYNAMICS CONCEPTS

The boundary layer of a fluid is the area where this movement is disturbed by the presence of a solid with which it is in contact. The boundary layer is defined as one in which the velocity of the fluid moving with respect to the solid varies from zero to 99% of the velocity of flow is not disturbed.

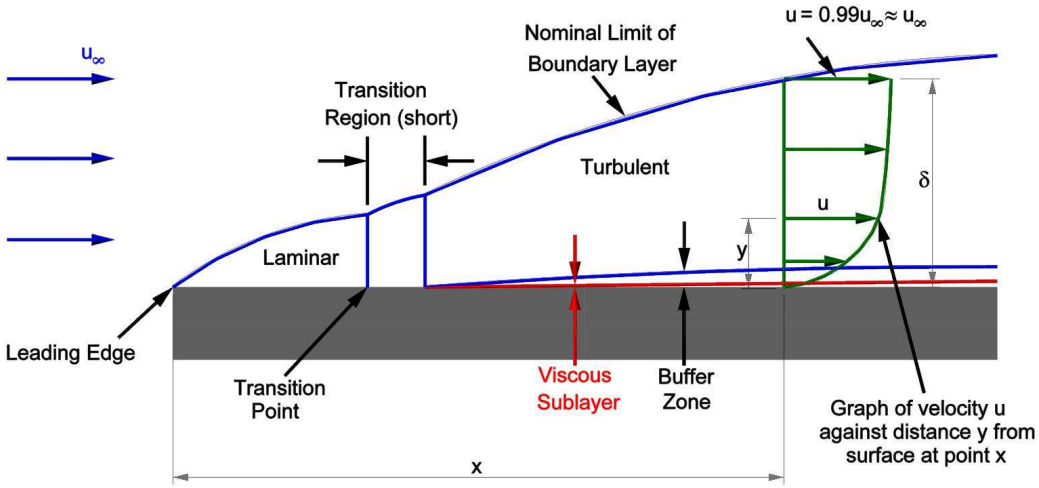

Figure 26. Boundary layer properties.

As more fluid is slowed because of the viscous forces the boundary layer thickens. Initially the boundary layer includes only laminar flow but as the boundary layer thickness increases the laminar layer loses stability and the flow becomes less even. The point at which the laminar flow starts to deteriorate is called the transition point and is at the start of a region called the transition region where the flow changes from laminar flow to turbulent flow.

The **Reynolds number** is a very important parameter when analysing these kinds of flows, as the performance of airfoils can be very sensitive to the magnitude of this parameter, and especially to the location of the transition between laminar and turbulent flow:

$$Re = \frac{U \cdot L}{\nu} = \frac{\rho U L}{\mu} = \frac{Inertial\ force}{Viscous\ force} \qquad \text{[Equation 2]}$$

Where, ρ is the fluid density, μ is fluid viscosity, ν=μ/ρ is the kinematic viscosity and U and L are a velocity and length that characterize the scale of the flow.

Sometimes it is useful that the boundary layer is turbulent. In wind turbines, are chosen more often airfoils that generate a turbulent boundary layer, as it remains adhered profile at higher angles of attack than the laminar boundary layer, thus preventing the profile from

stalling, that is, stop generating aerodynamic lift abruptly by the detachment of the boundary layer.

Separation is when the flow no longer manages to stay attached to the surface. When this happens, there will be a layer of reversed flow close to the surface, while the oncoming flow will be pushed away from the surface. In between the reversed and non-reversed flow, there will be an area of irregular flow. The area downstream of the separation point will have an almost uniform pressure, which will be nearly the same as the pressure at the separation point. The oncoming air flows over both the airfoil and the separation bubble, in effect flowing past a body of a completely different shape. This can reduce lift and increase drag dramatically. When a wing is being heavily affected by stagnation, and subsequent separation, it is said that the wing is in the stall area. This is usually visible as a shift in direction for the lift and drag curves of airfoils. If the progress of the separation occurs rapidly, the shift can be very sudden and dramatic.

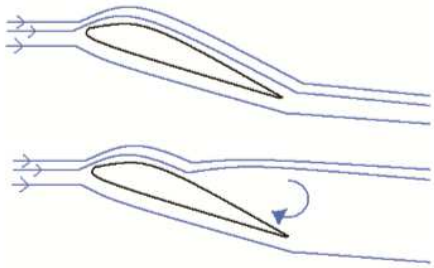

Figure 27. Attached flow (upper) and separated flow (lower).

As the air flows across the airfoil, it will be accelerated over the first part (negative pressure gradient), and it will be decelerated over the last part (positive pressure gradient). With a negative pressure gradient, separation is not a problem. With a positive, or adverse, pressure gradient, the risk of separation is big, as the air is flowing towards an increasing pressure. If the increase in pressure it faces is too big, the flow will get pushed away from the surface. The problem with separation is therefore mainly on upper surface at the back of the airfoil.

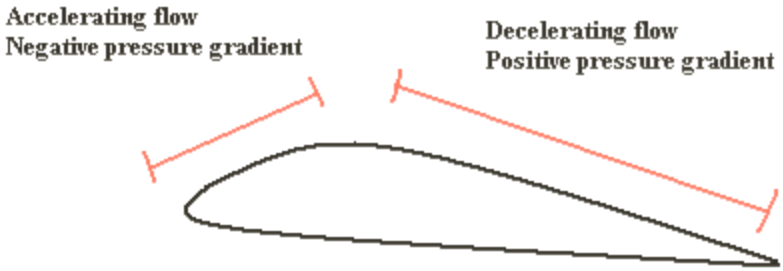

Figure 28. General flow patter over airfoil.

Therefore, it is necessary to design the backside of the upper surface with great care to avoid unwanted separation.

5.1. LAMINAR VS. TURBULENT FLOW

Airfoils are very sensitive to whether the flow is laminar or turbulent, as these two flow types possess very different qualities in terms of friction, boundary layer growth and tendency to separation. It is known from general fluid mechanics that the flow along a plate will usually start laminar, and then turn turbulent once the Reynolds number reaches a critical value. For a big wing, this might mean that it will have laminar flow over the front, and then have the flow turn turbulent further back on the wing. This means there will be two types of flow present with very different qualities, and the transition point where the change occurs, will not be a fixed point.

In laminar flow, the streamlines will be smooth. The tension in the boundary layer comes from layers of fluid moving over each other, and the particles tend to stay in the same layer.

In turbulent flow, the fluctuations cause the particles to get mixed and move through the layers. This causes the flow to be a more random mixture of particles of high and low kinetic energy, giving a much more uniform velocity profile.

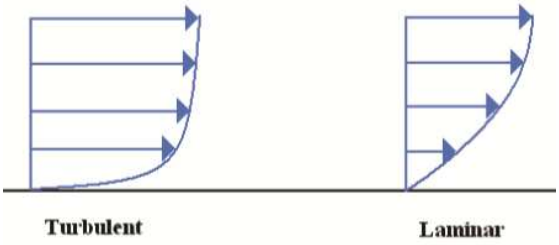

Figure 29. Illustration of the velocity fields of laminar and turbulent flow.

Two of the most distinct differences in effect between laminar and turbulent flow is that turbulent flow has higher friction and lower tendency to separate. The reason for these qualities is clearly visible by looking at figure 29. It can be seen that turbulent flow has far higher velocity close to the surface compared to laminar flow. It is also known that separation occurs when the velocity at the surface drops below zero as it can be seen in the figure 30. Therefore, having a higher velocity close to the surface means it will take a higher pressure gradient to reduce the flows velocity to zero, thus the lower tendency to separate in turbulence flow.

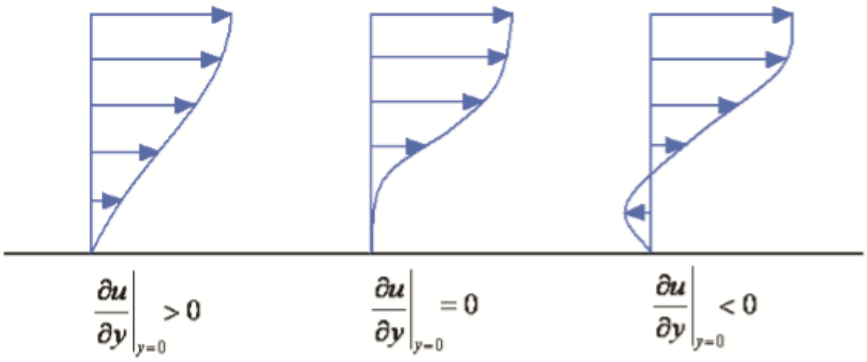

Figure 30. Illustration of flow field for attached flow (left), on the verge of separating (middle), and separated flow (right).

This basic knowledge is used to improve performance in all sorts of applications, the most famous example being golf balls, which are dimpled to trigger turbulent flow, causing the flow to separate further back on the ball, thus resulting in less overall drag.

An aerodynamic phenomenon known as stall should be considered carefully in turbine blade design. Stall typically occurs at large angles of attack depending on the aerofoil design. The boundary layer separates at the tip rather than further down the aerofoil causing a wake to flow over the upper surface drastically reducing lift and increasing drag forces. This condition is considered dangerous in aviation and is generally avoided. However, for wind turbines, it can be utilised to limit the energies maximum power output to prevent generator overload and excessive forces in the blades during extreme wind speeds and could also occur unintentionally during gusts. It is therefore preferable that the onset of the stall condition is not instantaneous for wind turbine aerofoils as this would create excessive dynamic forces and vibrations.

5.2. LIFT JUSTIFICATION

Lift and Drag forces are important parameters in a wind turbine system because these parameters decide the efficiency of the wind turbine. More energy can be extracted from wind using lift rather than drag, but this requires specially shaped airfoil surfaces. The airfoil shape is designed to create a differential pressure between the upper and lower surfaces, leading to a net force in the direction perpendicular to the wind direction.

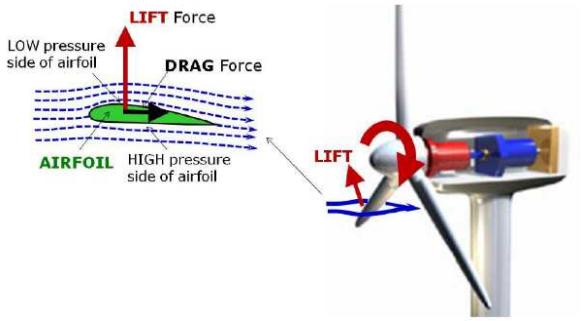

Figure 31. Lift wind turbine concept.

The justification of lift force can be explained by two theories:

5.2.1. Newton

The fact that the air is forced downward clearly implies that there will be an upward force on the airfoil as a Newton's 3rd law reaction force. From the conservation of momentum viewpoint, the air is given a downward component of momentum behind the airfoil, and to conserve momentum, something must be given an equal upward momentum.

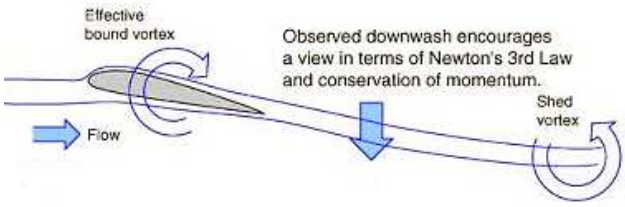

Figure 32. Newton´s 3rd law reaction force.

5.2.2. Bernoulli

Due to the geometry of the profile relative to its current position, the fluid velocity increases at the top and at the bottom is reduced. Bernoulli's equation therefore concludes that the wing gets "sucked" upward by the reduced pressure.

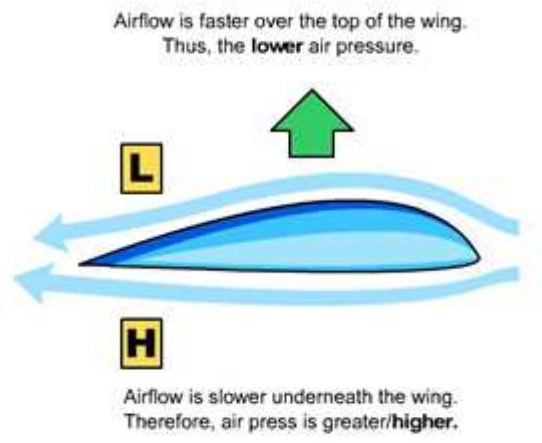

Figure 33. Pressure distribution.

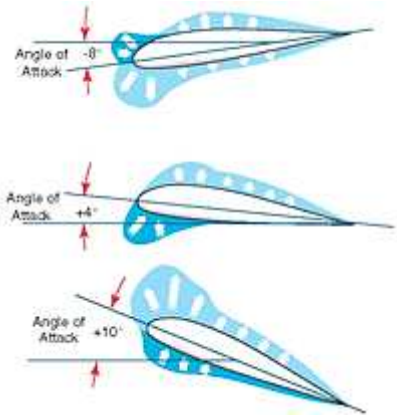

Figure 34. Pressure distribution according to the angle of attack.

It can be seen in the Figure 34 to the right that as the angle of attack is increased, as in the bottom picture, the resultant force from the deflection of the air both above and below the wing is also a major component to lift.

5.3. AERODYNAMICS FORCES AND PARAMETERS

The resultant forces on an airfoil depend on its relative position which is determinate by the angle of attack (α) that is defined as the angle between the chord line of the blade and the vector representing the oncoming flow. The figure below shows the resultants forces, wind speed vectors and relative position´s angles on an airfoil section.

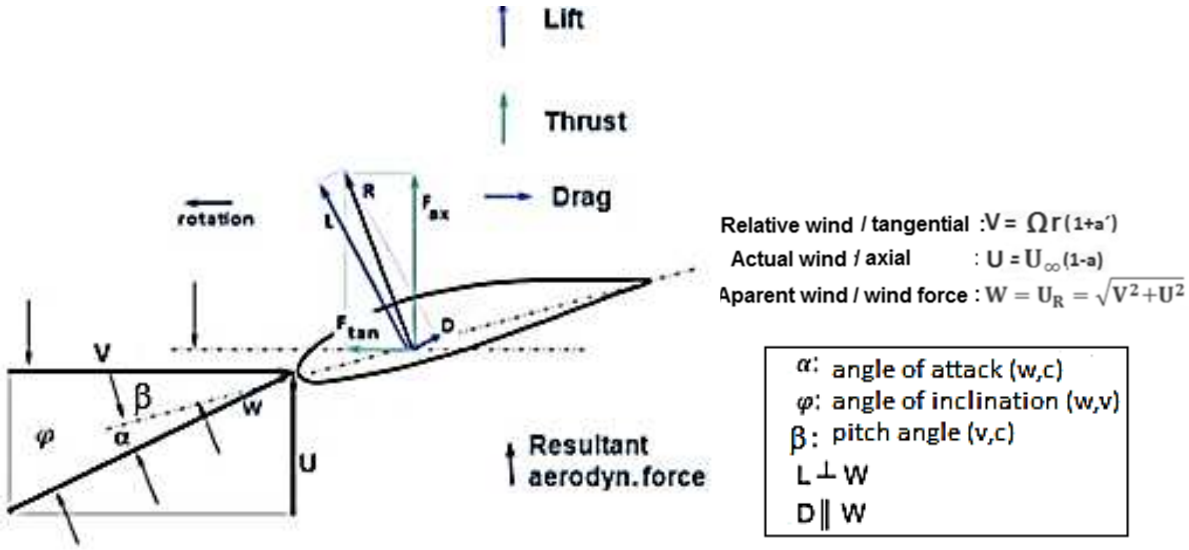

Figure 35. Airfoil section.

More specifically, **lift** on a body is defined as the force on the body in a direction normal to the flow direction. Lift will only be present if the fluid incorporates a circulatory flow about the body. The velocity above the body is increased and so the static pressure is reduced. The velocity beneath is slowed down, giving an increase in static pressure. So, there is a normal force upwards called the lift force expressed by:

$$L = \frac{1}{2} c_L \rho A w^2 \qquad \text{[Equation 3]}$$

The **drag** on a body in an oncoming flow is defined as the force on the body in a direction parallel to the flow direction. For a win turbine to operate efficiently the lift force should be high and drag force should be low. For small angles of attack, lift force is high and drag force is low. If the angles of attack (α) increases beyond a certain value, the lift force decreases and the drag force increases. So, the angle of attack plays a vital role. Drag force is obtaining from the following formula:

$$D = \frac{1}{2} c_D \rho A w^2 \qquad \text{[Equation 4]}$$

Pitching moment is defined to be about an axis perpendicular to the airfoil cross-section.

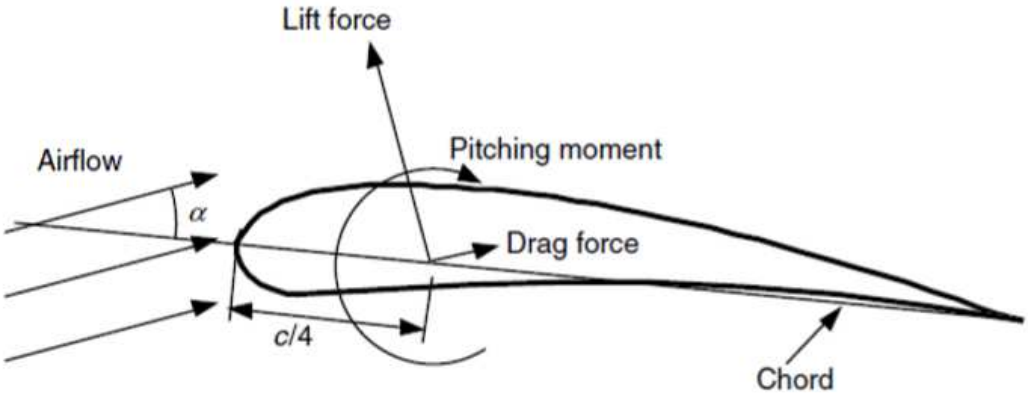

Figure 36. Resultant components on an airfoil.

Force and moment coefficients, which are function of Reynolds number, can be defined for two or three dimensional objects. In two dimensional cases, the forces measured are forces per unit span. Rotor design usually uses two-dimensional coefficients, determinate for a range of angles of attack and Reynolds number, in wind tunnel test. The two dimensional **lift coefficient** is defined as:

$$C_L = \frac{L/l}{\frac{1}{2}\rho U^2 c} = \frac{Lift\ force/unit\ length}{Dynamic\ force/unit\ length}$$ [Equation 5]

The two-dimensional **drag coefficient** is defined as:

$$C_D = \frac{D/l}{\frac{1}{2}\rho U^2 c} = \frac{Drag\ force/unit\ length}{Dynamic\ force/unit\ length}$$ [Equation 6]

And the **pitching moment coefficient** is:

$$C_M = \frac{M}{\frac{1}{2}\rho U^2 c} = \frac{Pitching\ moment}{Dynamic\ moment}$$ [Equation 7]

Where ρ is the density of air, U is the velocity of undisturbed airflow, c is the airfoil chord length and l is the airfoil span.

One very important parameter for all types of rotodynamic machines is the **tip speed ratio** (TSR), λ, which is the ratio of the translational speed at the tip of the blade to the velocity of the free stream of fluid:

$$\lambda\ (\mathrm{TSR}) = \frac{\Omega \cdot R}{V}$$ [Equation 8]

where u is the blade tip speed, and Ω and R are the angular velocity and the radius of the turbine rotor, respectively.

Aspects such as efficiency, torque, mechanical stress, aerodynamics and noise should be considered in selecting the appropriate tip speed. The efficiency of a turbine can be increased with higher tip speeds, although the increase is not significant when considering some penalties such as increased noise, aerodynamic and centrifugal stress.

Finally, the **power coefficient** is defined as:

$$C_P = \frac{P_{rotor}}{\frac{1}{2}\rho A U^3} = \frac{Rotor\ power}{Dynamic\ power}$$ [Equation 9]

where A is the projected airfoil area (chord x span).

The lift and drag coefficients C_L and C_D are functions of the angle of attack (α) and the shape of the airfoil. For a typical airfoil they look as in the figure below:

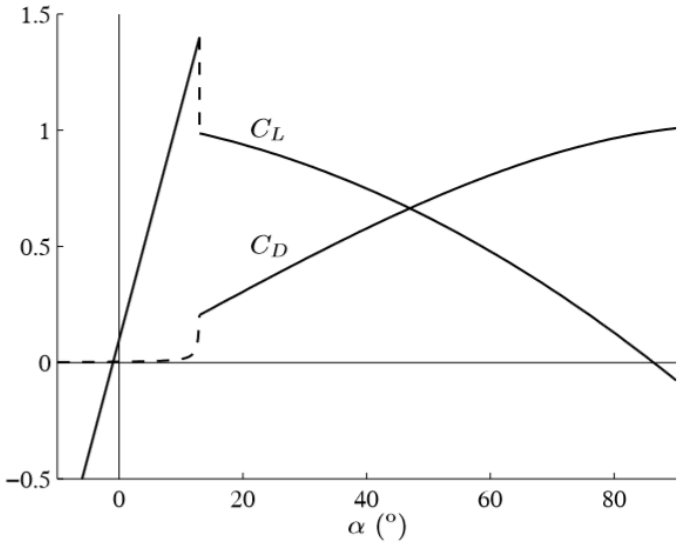

Figure 37. Typical lift and drag coefficients as function of angle of attack of an airfoil.

For low angles of attack, it is observed that C_L increases in pro-portion to α whereas C_D remains almost constant and very low. However, an abrupt change occurs at α= 13º. When the incidence angle exceeds this critical value, the airf ow is no more laminar and separates from the upper side of the airfoil. This yields a differential pressure that reduces the lift and increases the drag. Under these conditions, it is said that the airfoil stalls.

5.4. AIRFOIL TERMINOLOGY

Airfoils are structures with specific geometric shapes that are used to generate mechanical forces due to the relative motion of the airfoil and a surrounding fluid. Wind turbine blades use airfoils to develop mechanical power. The cross-sections of wind turbine blades have the shape of these airfoils. The width and length of the blade are functions of the desired aerodynamic performance, the maximum desired rotor power, the assumed airfoil properties, and strength considerations.

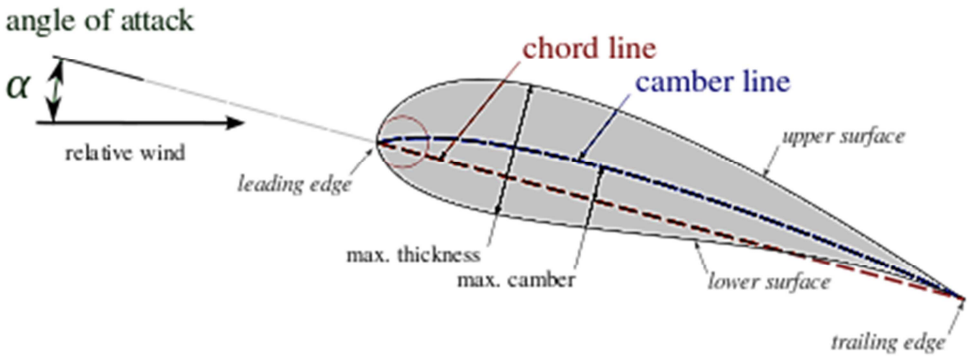

Figure 38. Airfoil nomenclature.

The mean camber line is the locus of points halfway between the upper and lower surfaces of the airfoil. The most forward and rearward points of the mean camber line are on the leading and trailing edges, respectively. The straight line connecting the leading and trailing edges is the chord line of the airfoil, and the distance from the leading to the trailing edge measured along the chord line is designated the chord, c, of the airfoil.

The camber is the distance between the mean camber line and the chord line, measured perpendicular to the chord line. The thickness is the distance between the upper and lower surfaces, also measured perpendicular to the chord line. Finally, the angle of attack, α, is defined as the angle between the relative wind and the chord line.

National Advisory Committee for Aeronautics (NACA) four and five digit designs have been used for early modern wind turbines. The classification shows the geometric profile of a NACA aerofoil where the 1st digit refers to maximum chamber to chord ratio, 2nd digit is the camber position in tenths of the chord and the 3rd & 4th digits are the maximum thickness to chord ratio in percent. Regarding the NACA-4 profiles, there are basically three families used in wind turbines.

First the 00XX profiles, especially the 0015, are having a completely symmetrical profile but they are use basically for vertical axis wind turbines.

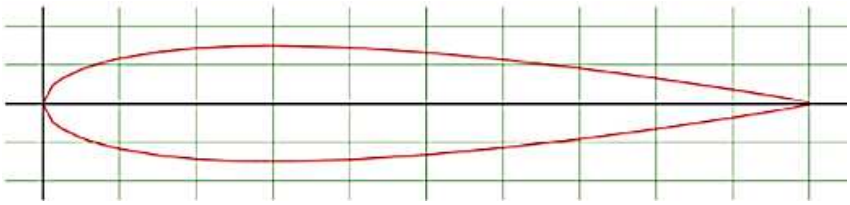

Figure 39. NACA 0015.

The second family would be the 4-digit NACA 24XX-type profiles. These profiles are very versatile and are used for different uses, they work with low Reynolds and their

relation C_L/C_D is good. Non-submission convex faces, makes it a candidate to manufacture simple.

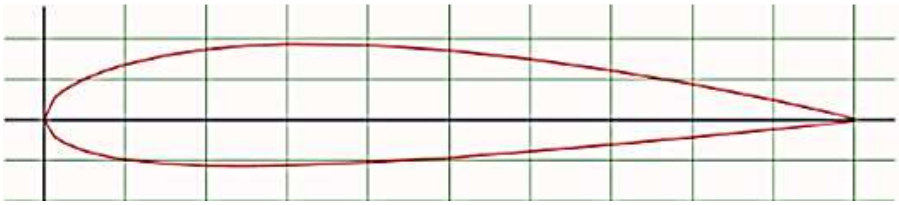

Figure 40.NACA 2415.

The third major in the 4-digit NACA-profiles are the 44XX family. These profiles are used in small wind turbines because of their high C_L/ C_D, so they are a good alternative. But the design of their concave shape makes manufacture of the profile is more costly.

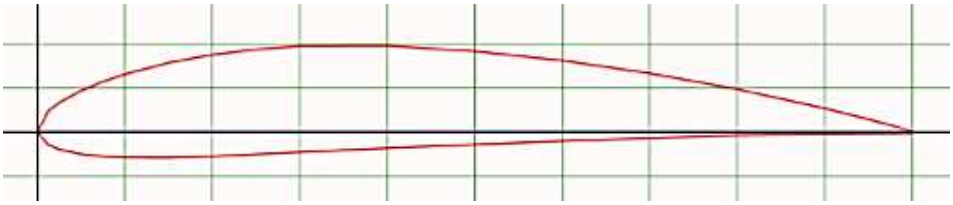

Figure 41. NACA 4412.

Within the NACA-5 profiles figures are also two important families used in wind turbines. First the 23-0XX, series of very similar to 44XX characteristics but biconvex symmetrical profiles which cause them to have a more complex geometry, by contrast have a C_L/C_D slightly higher than 44XX series.

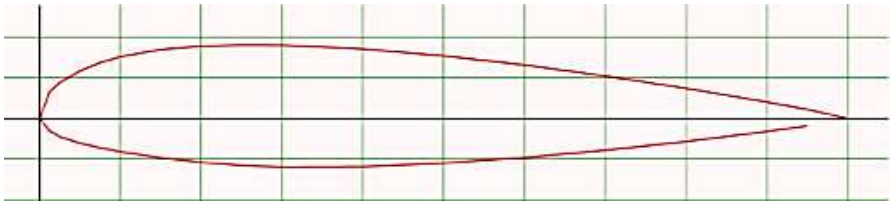

Figure 42. NACA 2305.

The second family is the 6X-2XX. But its features are more conducive to wind turbines with diameters bigger than 20m, and therefore this profile has extended its use in wind turbines of medium and high power, not the mini-turbines.

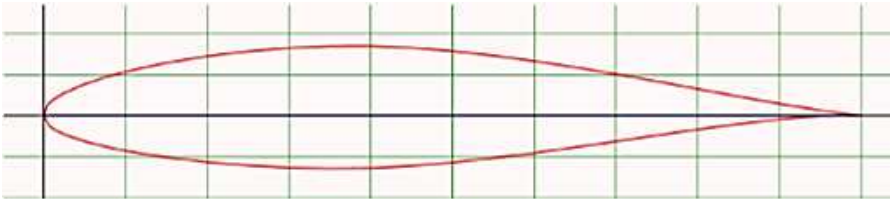

Figure 43. NACA 64-215.

6. WIND POWER EXTRACTION

The wind originates naturally due to differences in surface temperature. This wind, by the fact of moving has energy, which is a consequence of the kinetic energy of moving air particles. This **kinetic energy** is expressed as:

$$E_c = \frac{1}{2} m v_1^2 \qquad \text{[Equation 10]}$$

In turn, the mass of the particles of air passing through a certain section, perpendicular to the wind direction is:

$$m = \rho A l \qquad \text{[Equation 11]}$$

As a result the kinetic energy that passes through a section is obtained from the following formula:

$$E_C = \frac{1}{2} \rho A l v_1^2 \qquad \text{[Equation 12]}$$

The **power available** in the wind is the wind kinetic energy per time unit. It can be obtained by the product of the kinetic energy per v/l.

$$P_a = \frac{E_C}{t} = \frac{1}{2} \rho A l v_1^2 \frac{v_1}{l} = \frac{1}{2} \rho A v_1^3 \qquad \text{[Equation 13]}$$

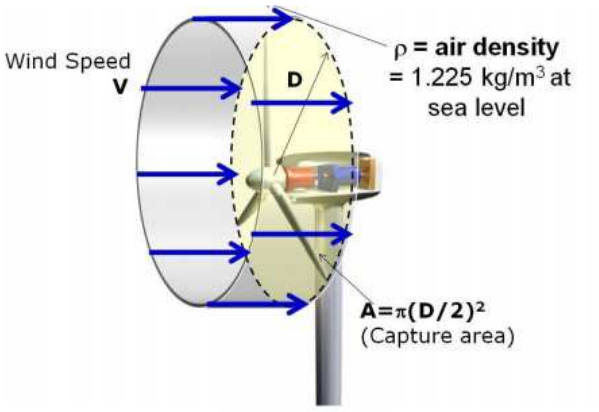

Figure 44. Power available from the wind.

Only a portion of the power may be picked up by the rotor blades. Therefore the **captured power** is:

$$P_c = C_P P_a = C_P \frac{1}{2} \rho A v_1^3 \qquad \text{[Equation 14]}$$

Where C_P is the power coefficient that indicates the ability of the blades to capture energy from the wind.

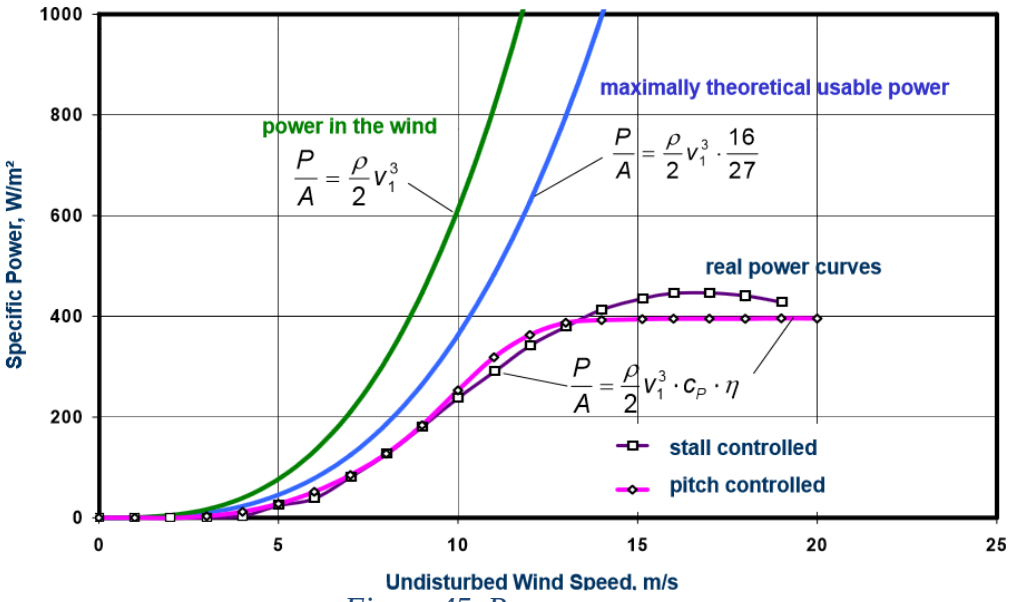

Figure 45. Power curve.

6.1. BELTZ´S LAW

A physical limit exists to the quantity of energy that can be extracted, which is independent of design. The energy extraction is maintained in a flow process through the reduction of kinetic energy and subsequent velocity of the wind. The magnitude of energy harnessed is a function of the reduction in air speed over the turbine. 100% extraction would imply zero final velocity and therefore zero flow. The zero flow scenario cannot be achieved hence all the winds kinetic energy may not be utilised. This principle is widely accepted and indicates that wind turbine efficiency cannot exceed 59.3%. This parameter is commonly known as the power coefficient Cp, where max Cp = 0.593 referred to as the Betz limit.

Albert Betz published between 1922 and 1925 that, by applying elementary physical laws, the mechanical energy extractable from an air stream passing through from a given cross-sectional area is restricted to a certain fixed proportion of the energy or power contained in the air stream.

This fixed proportion is represented by a value of the power coefficient CP, the ratio of the extractable mechanical power to the power contained in the air stream.

Fig. 45. Shows the stream tube where U1 is the undelayed free-stream velocity, the wind speed, before it reaches the converter, whereas U2 is the flow velocity far behind the converter.

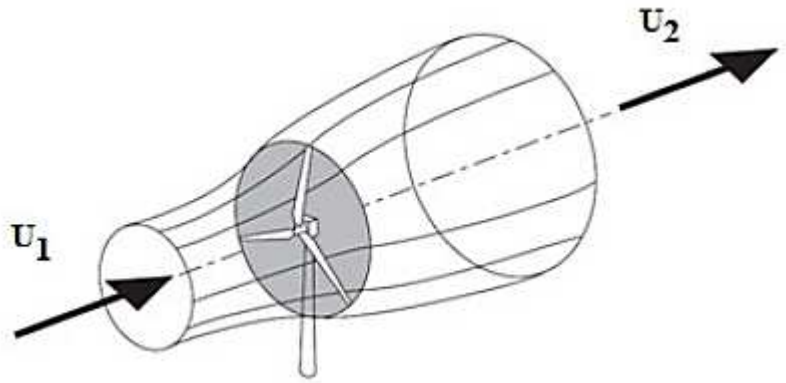

Figure 46 Stream tube.

Fig. 46 shows the ideal power coefficient versus the flow speed ratio of the flow before and after the energy converter. This graphic allows to note that the maximum power coefficient occurs at a velocity ratio U2/U1 = 0.333.

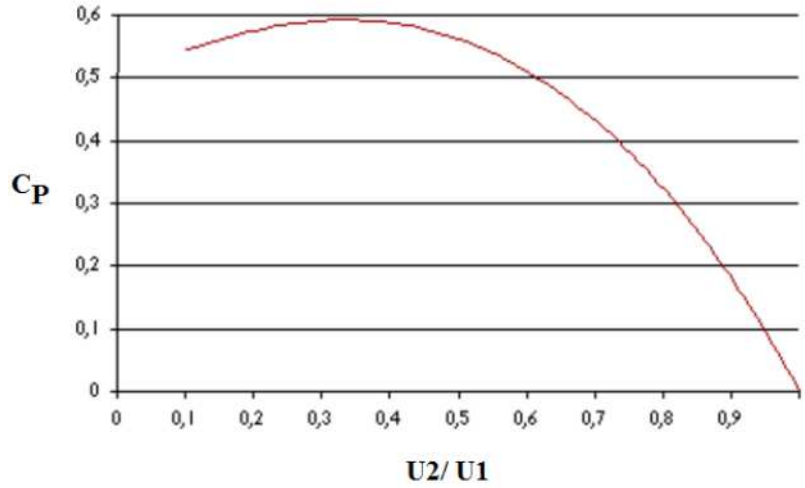

Figure 47 Ideal power coefficient versus the flow speed ratio U2/U1.

The Betz theory assumes constant linear velocity. Therefore, any rotational forces such as wake rotation, turbulence caused by drag or vortex shedding (tip losses) will further reduce the maximum efficiency. Efficiency losses are generally reduced by:

- Avoiding low tip speed ratios which increase wake rotation
- Selecting aerofoils which have a high lift to drag ratio
- Specialised tip geometries

6.2. POWER COEFFICIENT

The power coefficient, correspondingly the max power coefficient, can generally be expressed as a function of TSR (λ) which combines the most important design variables, so that the behaviour of any propeller is fully defined to represent the power coefficient as a function of the speed ratio λ.

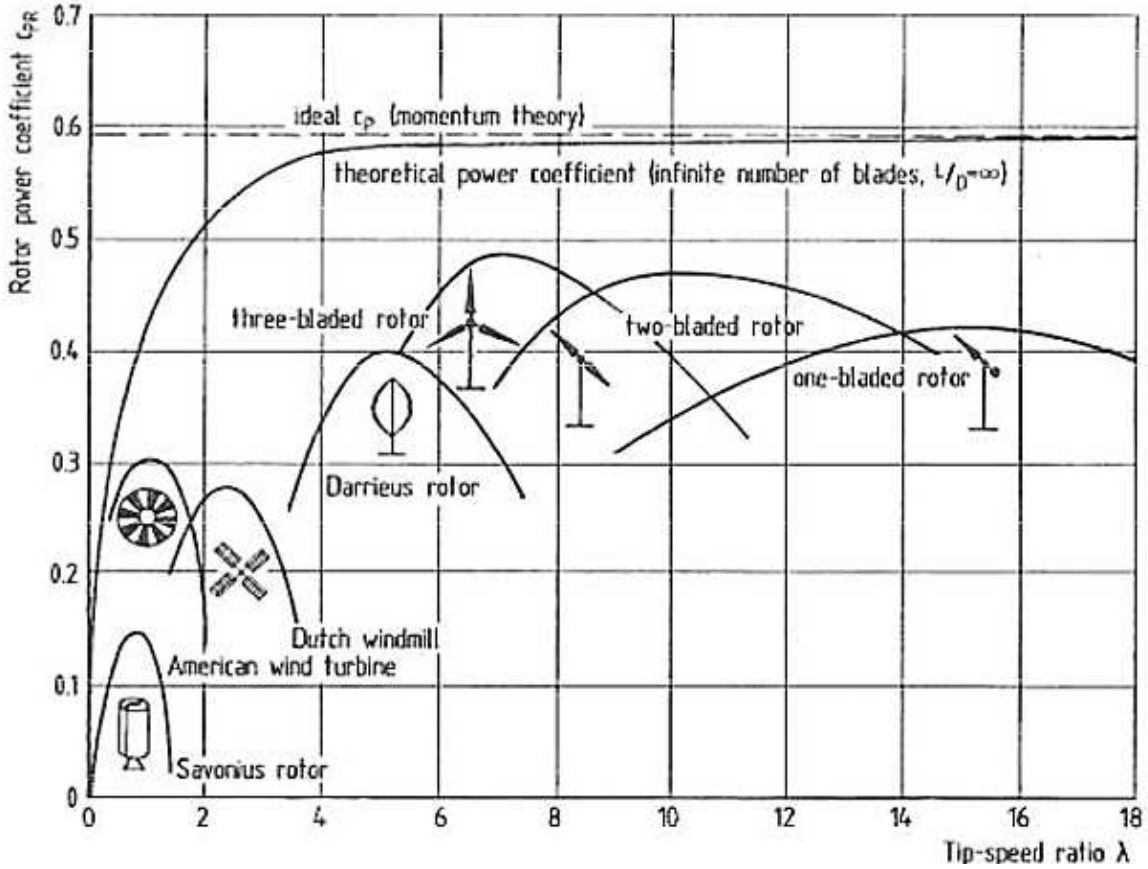

Figure 48. Cp vs λ.

In the design of a propeller many variables it is often necessary to estimate the coefficient of maximum power that can be obtained for a configuration. To enable this estimate on the basis of numerous experimental data, in 1976 Wilson proposed the following equation to calculate the value:

$$Cp_{máx} = 0.593\,[\frac{\lambda\, B^{0.67}}{1.48 + (B^{0.67} - 0.04)\lambda + 0.0025\lambda^2} - \frac{1.92\,\lambda^2\, B\, C_D}{1 + 2\lambda\, B\, C_L}] \quad \text{[Equation 15]}$$

Where B is the number of blades, λ is the tip speed ratio, CD is the drag coefficient and CL the lift coefficient. This parameter can also be showed in graphics like this to three-bladed wind turbines:

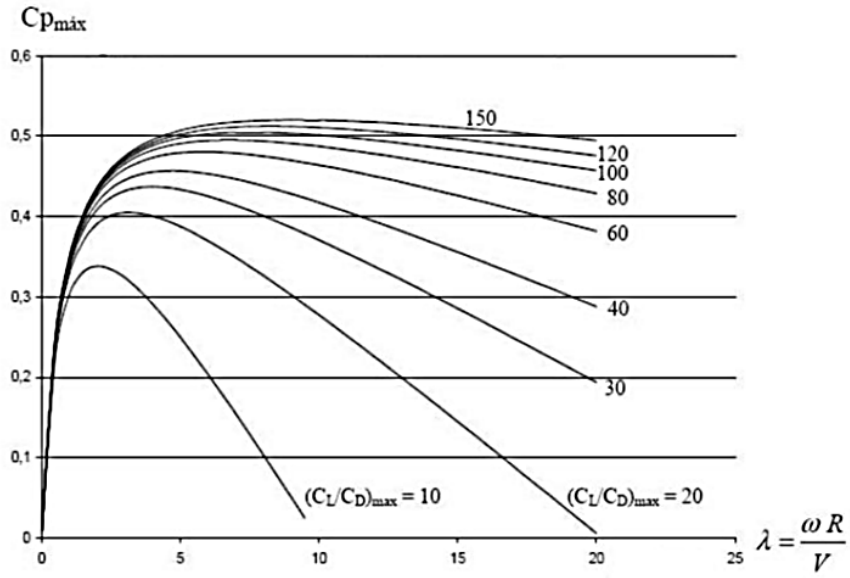

Figure 49. Cp_{max} vs λ as function of C_L/C_D.

Most wind turbines use two or three blades and, in general, most two-bladed wind turbines use a higher TSR than most three-bladed wind turbines. Thus, there is little practical difference in the maximum achievable Cp.

In the figure below, can be seen difference Cp between two-bladed and three-bladed designs, assuming no drag.

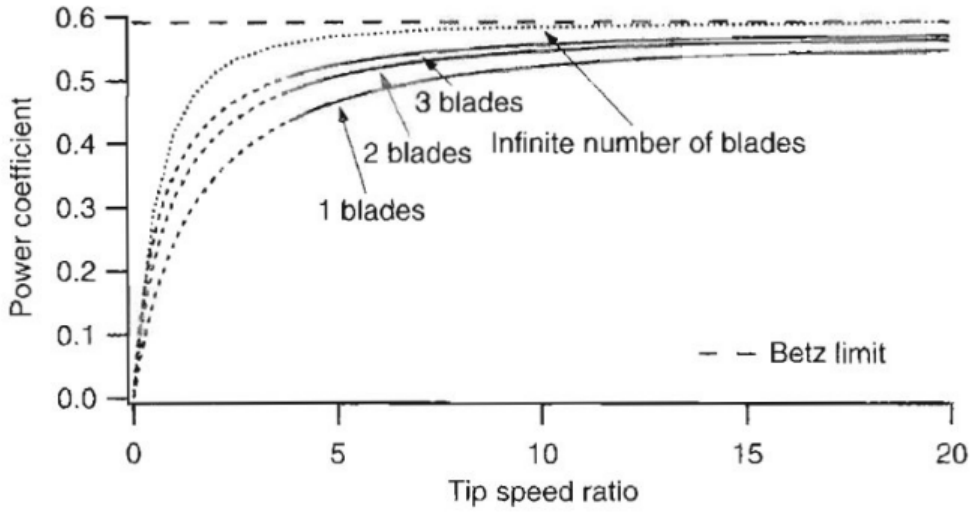

Figure 50. Maximum Cp achievable as a fucntion of number of blades, no drag.

In the next figure is shown the effect of the lift to drag ratio on maximum achievable power coefficients for the three-bladed rotor. There is a clearly significant reduction in maximum achievable power as the airfoil drag increases.

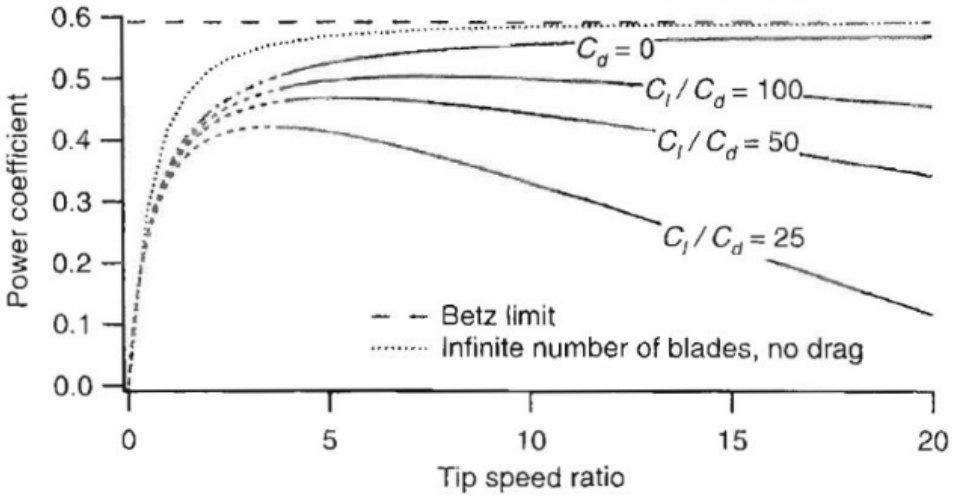

Figure 51. Maximum Cp achievable of a three-blade optimum rotor as a function of the lift to drag ratio.

It can be seen that is clearly benefits the blade designer to use airfoils with high lift to drag ratios. Practical rotor power coefficients may be further reduced as a result of non-optimum blade designs that are easier to manufacture.

7. MODELING IN ANSYS

7.1. INTRODUCTION

Recent approaches that study the dynamic response of wind turbines are based largely on hybrid models comprised of concentrated and distributed parameters. The nacelle, the power-train subsystem and the generator are considered as systems with lumped parameters, while the blades and the tower are considered as systems with uniformly distributed mass, elastic and damping characteristics.

In this study, three models are developed and compared:

- **Model 1**: Mechanical 2D analysis represented by a mathematical system, solve by FEM and a MATLAB program based on Newmark method.
- **Model 2**: 3D Mechanical model generated in Mechanical branch of Ansys.
- **Model 3**: 3D wind turbine modelled in Solidworks.

A transient analysis is made using model 3 in CFD with a specific pitch angle and considering the tower shadow. To realise this analysis some input and fluid domain parameters are been considered. Finally, the pressure distribution obtained is used to obtain the loads which to apply in the models to calculate displacements and strains.

Depending on the study objective, various degrees of freedom of the model could be removed, i.e. simplifying assumptions are introduced so as to arrive more quickly and effectively to the final solution. In Figure 64, the wind turbine model does not account for the influence of the wind flow on the tower. The main attention is paid to the wind force applied as a concentrated force at the top of the tower. Only the maximum loads, acting on the system, are considered. Any changes in the wind direction and intensity are not taken into account.

The model 1 in Figure 52 is based again on lumped masses (nacelle, generator) and distributed masses (blades, shafts, tower). The elasticity of the tower is studied in two planes – by considering the fore-aft and side vibrations. Each of the two in-plane vibrations considers up to the second natural vibration mode. A method for linearization of the system - analytical and numerical is presented.

A method for optimizing the load-bearing structure of the wind turbine is discussed. The prime model of the tower is constructed as an equivalent cantilever beam made up of

sections with identical cross-sections. The beam deflections are measured neglecting any secondary effects such as axial and shear loads. Laminar air flow is adopted.

The tower and the blades dynamic response is studied in figure 67 and 68. The tower and blades are studied simultaneously, using the finite element method [14] or the method of the modal analysis.

7.2. MODELLING THE HAWT

7.2.1. Models definition

The different developed and compared models are detailed in this section:

- **MODEL 1**

Figure 52 shows the system model of a downwind and tilt angle HAWT. The wind first reaches the tower and then the blades.

The scheme accounts for the tower, the nacelle and the blades. It is assumed that the tower (T) and the blades (B) are systems with distributed parameters, where:

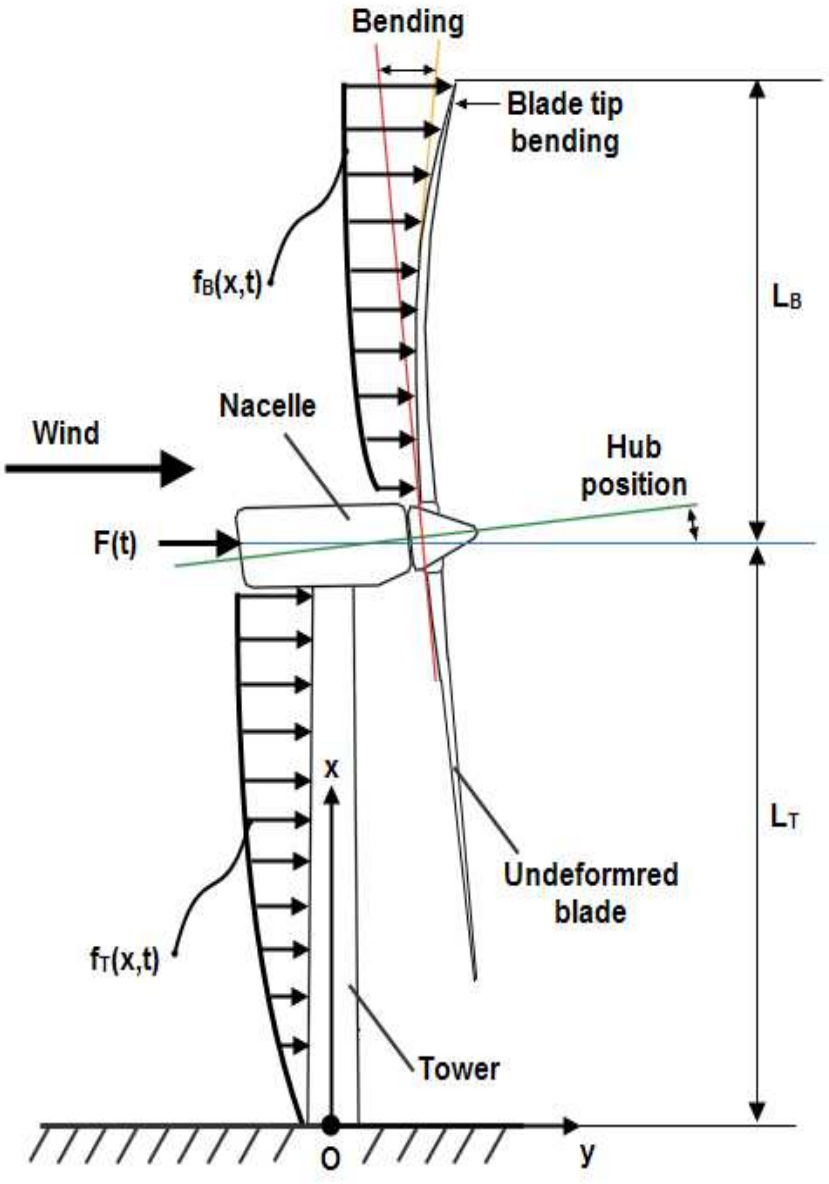

Figure 52. HAWT system model

E_T, E_B - elasticity moduli; J_T, J_B - moments of inertia;

m_T, m_B - distributed mass ; C_T, C_B - damping;

L_T, L_B - length.

The nacelle is considered as a concentrated mass M_N.

Under the action of the wind on the behaviour of the system axis y, can be described by the following partial differential equation (PDE):

[Equation 16]

$$E(x)J(x)\frac{\partial^4 w(x,t)}{\partial x^4}+m(x)\frac{\partial^2 w(x,t)}{\partial t^2}+C(x)\frac{\partial w(x,t)}{\partial t}=f(x,t)+F(t)\delta(x-h)$$

The designations are:

EJ - flexural rigidity; $\delta(x-h)$ - Dirac δ-function; $w(x,t)$ displacement;

, where $x\in[0;L];L=L_T+L_B;\ \ t\geq 0$.

[Equation 17]

$$x\in[0;L_T)\Rightarrow\begin{cases}E(x)=E_T;J(x)=J_T(x);\\ m(x)=m_T(x);\\ f(x,t)=f_T(x,t);\end{cases}\qquad x\in(L_T;L]\Rightarrow\begin{cases}E(x)=E_B;J(x)=J_B(x);\\ m(x)=m_B(x);\\ f(x,t)=f_B(x,t);\end{cases}$$

where $f_T(x,t)$ and $f_B(x,t)$ is the distributed wind load, acting respectively on the tower and on the blades; $F(t)$ - a concentrated force that accounts for the wind load acting on the nacelle and on the rotor disk.

When x = L_T, it is assumed that

- the tower and blade are in contact;
- to concentrated mass M_N of the nacelle is located
- $f(L_T,t)=f_T(L_T,t)=f_B(L_T,t)$ and $\frac{\partial w}{\partial x}(x=L_T,t)=0$

The boundary conditions are:

$$\left|\begin{array}{l} w(x=0,t)=0 \\ \dfrac{\partial w}{\partial x}(x=0,t)=0 \end{array}\right. \qquad \left|\begin{array}{l} \dfrac{\partial^2 w}{\partial x^2}(x=L,t)=0 \\ \dfrac{\partial^3 w}{\partial x^3}(x=L,t)=0 \end{array}\right. \qquad \text{[Equation 18]}$$

The initial conditions are:

$$w(x,0)=0;\ \dot{w}(x,0)=0\,. \qquad \text{[Equation 19]}$$

The following is assumed:

- the material of the tower and the blades is homogeneous, isotropic and obey the Hooke's law;
- the displacements are small, i.e. the dynamic behaviour is linear elastic ;
- the mass M_N does not rotate ;
- Rayleigh damping $[C]=\alpha[M]+\beta[K]$ is used for the beam, where α and β are coefficients that are determined by ξ - the percent modal damping

In this case, the response of the wind turbine is studied with fixed hub.

The solution of equation (16) under the specified assumptions and conditions (17), (18) and (19) is obtained by the use of the finite element method (FEM). The domain is meshed with beam type finite elements with cubic function as interpolation model. It follows for the stiffness matrix $\left[K^{(e)}\right]$ and the mass matrix $\left[M^{(e)}\right]$:

[Equation 20]

$$\left[K^{(e)}\right]=\frac{2EJ}{l^3}\begin{bmatrix} 6 & 3l & -6 & 3l \\ 3l & 2l^2 & -3l & l^2 \\ -6 & -3l & 6 & -3l \\ 3l & l^2 & -3l & 2l^2 \end{bmatrix};\quad \left[M^{(e)}\right]=\frac{\rho Al}{420}\begin{bmatrix} 156 & 22l & 54 & -13l \\ 22l & 4l^2 & 13l & -3l^2 \\ 54 & 13l & 156 & -22l \\ -13l & -3l^2 & -22l & 4l^2 \end{bmatrix}$$

A MATLAB program is developed to solve the finite element model of the mechanical system in Figure 521. The program is based on the numerical method of Newmark[1] and after a successful solution it reports the obtained **deformations and natural frequencies**. The model built and solved this way is further referred to as "basic equivalent model" or model1.

The developed mathematical model is compared with two 3-D models, developed in ANSYS and aimed at a more detailed examination of the wind turbine response, considering the wind load on the tower and blades.

- **MODEL 2**

3-D model similar to the above mentioned mathematical model 1, but has been expanded with the options of reporting the displacements and rotations of the wind turbine in the three orthogonal planes. In addition, it has been developed by the Mechanical branch of the Ansys software.

- **MODEL 3**

A second 3-D model, shown in Figure 53 and named model 3, is constructed with the CAD system SolidWorks.

[1] ***Newmark Method:*** *Implicit integration method used to solve differential equations used in numerical evaluations of the dynamic response of structures and solids such as Finite Element analysis to model dynamic systems.*

Figure 53. Model3 of the HAWT

The model 3 parameters are:

- **Tower**: tubular section (frustum of cone), wall thickness 12mm, materials - steel

$$L_T = 72\text{m};\ E_T = 2\times10^{11}\,\text{N.m}^2;$$
$$D_{T1} = 5\text{m}; D_{T2} = 2\text{m}; \rho = 7850kg/\text{m}^3;$$

D_{T1} and D_{T2} are the outer diameters at the tower tip and foundation respectively

- **Blade**: airfoil NACA0021, wall thickness 16mm, material - fiberglass [15]

$$L_B = 30\text{m};\ E_T = 4\times10^{10}\,\text{N.m}^2;$$
$$D_{B1} = 4\text{m}; D_{B2} = 1.5\text{m}; \rho = 1700kg/\text{m}^3;$$

D_{B1} and D_{B2} are the chords at the base and blade tip respectively

- **Nacelle**: concentrated mass of 20 tons

- **Rotor**: diameter = 74m

The wind turbine blades construction is based on the NACA0021 airfoil. It is a symmetric profile, a member of the family of four digit names, and is generated using the following relation [21]:

[Equation 21]

$$y = \frac{t}{0.2} c \left[0.2969 \sqrt{\frac{x}{c}} - 0.1260 \left(\frac{x}{c} \right) - 0.3516 \left(\frac{x}{c} \right)^2 + 0.2843 \left(\frac{x}{c} \right)^3 - 0.1015 \left(\frac{x}{c} \right)^4 \right]$$

where

c - chord length;

x - position on the chord from 0 to c;

y - half thickness at a given value of x;

t - maximum thickness as part of the chord ;

After applying the relationship [21] a set of XYZ coordinates of points are generated for corresponding sections that make up the profile. To achieve sufficient accuracy when modelling the blade and subsequently for its meshing, each section is made up of minimum of 100 points. Model 3 allows for studying the complex stress state at any point without any additional transfers to equivalent geometry.

7.2.2. Natural mode shapes and frequencies

A comparison is made between model 1, model 2 and model 3. The comparison uses results obtained from modal and transient analyses with pitch angle range $\beta\epsilon[4^o;17^o]$ and wind speed range $V_{wind}\ \epsilon[7;25]$m/s . It was found that in the range $\beta\epsilon[4^o;12^o]$, model 1 and model 2 are acceptable approximations of model 3, i.e. the response of the system is likely to be considered as 1-D. Some results of the modal analysis are shown below.

Figure 54 presents a comparison of the **first three natural mode shapes and frequencies** of model 2 and model 3, taking into account the tower, the nacelle and a single blade in vertical top position.

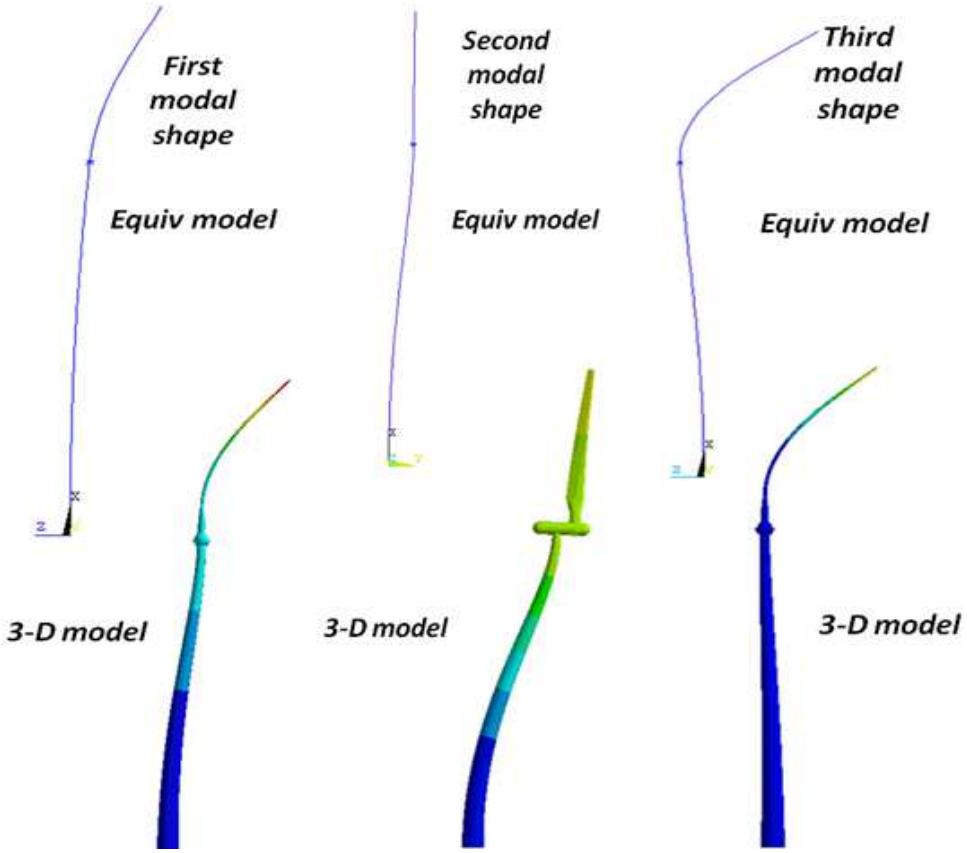

Figure 54. The first three natural mode shapes of model2 and model3

Table 2. Comparison between the first three natural frequencies of the models

Parameter	Model 3 A	Model 2 B	Model 1 C	Error, % B vs A	Error, % C vs B
1-st nat frequency [Hz]	0.793	0.801	0.813	1.01	1.49
2-nd nat frequency [Hz]	1.102	1.08	1.106	1.99	2.41
3-rd nat frequency [Hz]	4.116	4.148	4.393	0.78	5.91

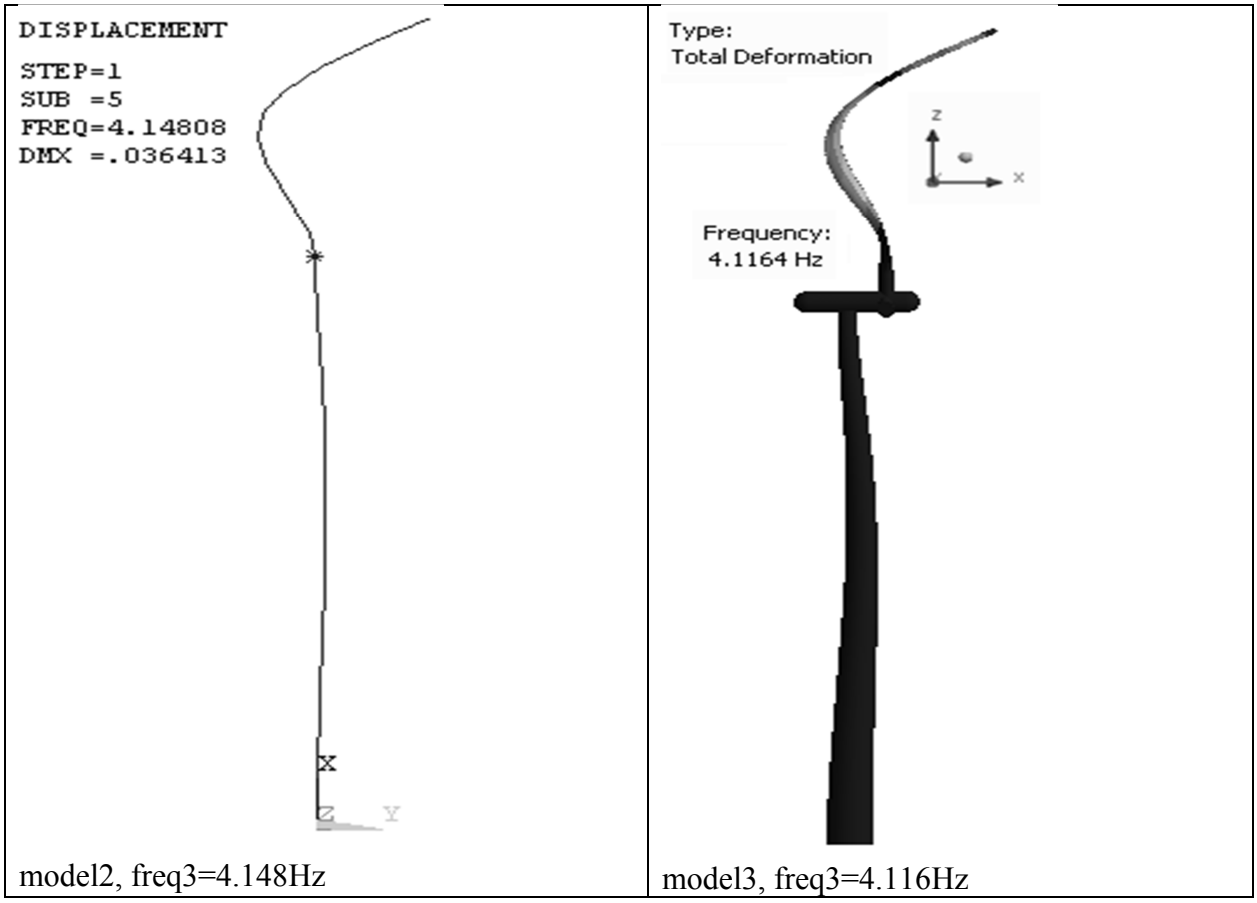

Figure 55. Model 2 vs Model 3, 3-rd natural frequency and mode shape at β=10°

Figure 55 shows a comparison in the **third natural frequency and mode shape** of model 2 and model 3. Compared are the natural frequencies of the blades, the tower and the nacelle in different model arrangements. It was found that model 1 and model 2 approximate with sufficient precision the frequency response of the 3-D components of the model 3.

7.2.3. Transient analysis

The transient analysis addresses the application of pulse wind loading, which lasts for 5 seconds. The load value is determined by CFD (computational fluid dynamics) simulations.

If the **lift coefficient** for an airfoil at a specified angle of attack is known (or estimated using a method such as thin-airfoil theory), then the lift produced for specific flow conditions can be determined using the equation below. This equation is used to generate the aerodynamic force caused by the wind and loading the tower.

$$F_L = \frac{1}{2}\rho_{air} v_x^2 A C_L \qquad \text{[Equation 22]}$$

where

F_L is the aerodynamic lift force

$\rho_{air} \approx 1.23$ kg/m^3 - air density at sea level

A- planform area

C_L- lift coefficient for a given angle of attack, Mach number and Reynolds number

The values of the lift coefficient may be taken from laboratory reports but very often, however, there is not enough data about the coefficients and the planform area at a given angle of attack. Therefore, the present study is carried out by the help of fluid simulations.

With the increase of the height $\boldsymbol{x}$, the wind speed varies according to the so-called Log-wind profile as follows:

$$v_x = \frac{v_{30}}{\kappa}\left[\ln\left(\frac{x-d}{x_0}\right)\right] \qquad \text{[Equation 23]}$$

where

$v_x\,[\mathrm{m/s}]$ is the horizontal wind speed at height $x\,[\mathrm{m}]$;

$v_{30} = 10\mathrm{m/s}$ - wind speed at a height of 30m,

x_0 - surface roughness ($x_0 = 0.03$ for grassland);

$\kappa \approx 0.41$ - the von Karman constant,

d - parameter accounting for the presence of additional barriers.

[Equation describes the vertical distribution of the horizontal wind speed. The rate of change of wind speed in height(x) is determinate as:

- xϵ [1; 60] m: the rate of change is significant and modelling by equation 23.
- xϵ [60; 100] m: the increase in v_x is 0.772m/s and it is possible to assume v_x (x > 60) = v_x (x =72) =11.27m/s, i.e. wind speed at hub of the turbine is almost constant.

For example, this equation can determinate wind speed of v_{30}=10m/s, i.e. wind at height of 30 meters.

Blade loading is also analysed for various values of β as well as for blade position in the tower shadow, Figure 58, and out of the tower shadow.

CFD (computational fluid dynamics) is a branch of fluid mechanics that applies numerical methods and algorithms to analyse problems related to fluid flows. The calculations are in most cases made by computers which simulate the interaction of liquids and gases with different surfaces and under certain boundary conditions.

The majority of the solved CFD problems are based on the Navier-Stokes equations, which describe each single-phase fluid flow. The equations represent the relationship between the speed, pressure, temperature and density of the moving fluid.

Using SolidWorks, the 3-D geometry of a fluid channel and a blade of the wind turbine inside the channel have been modelled. Subsequently, the geometry is transferred to the FEA (Finite Element Analysis) software ANSYS for research and analyses by the finite element method.

The ANSYS software is used to perform various CFD simulations with the constructed fluid channels by applying the same scaling parameters, so as to avoid errors in the results. For example, when studying a blade, the **fluid domain parameters** are set as follows:

- Re = 29.506×10^6 (Reynolds number)
- Subsonic flow (M << 1, M is the number of Mach)
- Continuous fluid
- Turbulence model = shear stress transport
- Heat transfer option = isothermal at 25°C
- Turbulence option = medium intensity at 5%
- Shear stress at the walls of the channel is zero, i.e. velocity of the fluid is not slowed down due to friction.

Figure 56 shows the summary report about the mesh and the physical parameters of the fluid simulation in Figure 57.

Mesh Report

Table 2. Mesh Information for Fluid Flow 07

Domain	Nodes	Elements	Tetrahedra
Default Domain	325025	1884696	1884696

Table 3. Mesh Statistics for Fluid Flow 07

Domain	Minimum Face Angle	Maximum
Default Domain	12.5845 [degree]	132.0

Physics Report

Table 4. Domain Physics for Fluid Flow 07

Domain - Default Domain	
Type	Fluid
Location	B44
Materials	
Air Ideal Gas	
Fluid Definition	Material Library
Morphology	Continuous Fluid
Settings	
Buoyancy Model	Non Buoyant
Domain Motion	Stationary
Reference Pressure	1.0000e+00 [atm]
Heat Transfer Model	Isothermal
Fluid Temperature	2.5000e+01 [C]
Turbulence Model	SST
Turbulent Wall Functions	Automatic

Figure 56. Summarized data about the finite element mesh and the physical parameters

The quality of the finite elements in the mesh is checked and over 85 % of the elements have element quality > 0.79, i.e. is the possibility of errors in the step of discretization is reduced.

Figure 57 presents the steps of the generation, verification and results output of a fluid simulation with NACA0021 blade at pitch angle of β=6°.

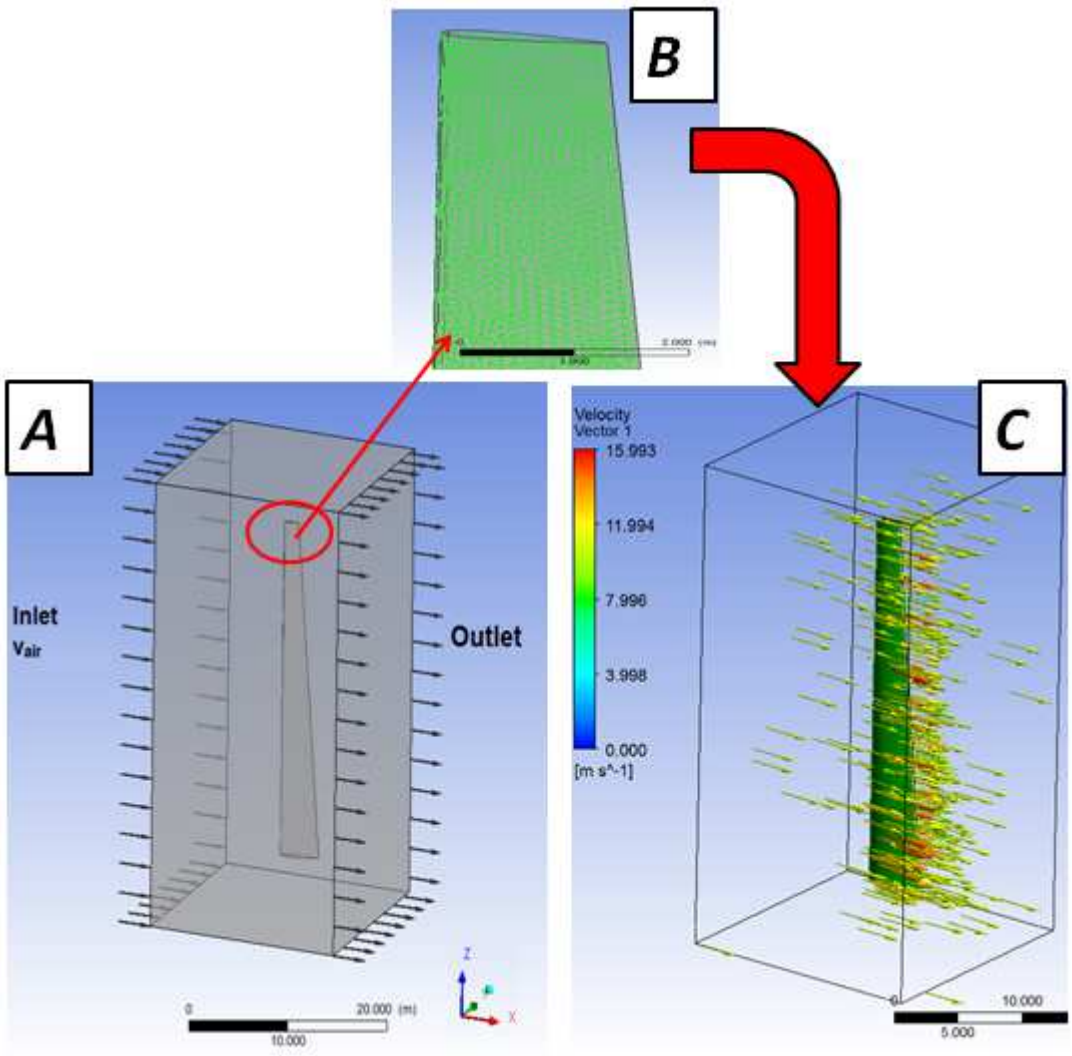

Figure 57. CFD simulation of a blade NACA0021, β=6°
A – Fluid channel with defined boundary conditions, B – Zoomed view of the finite element mesh near the blade tip, C – Fluid velocity variation around the blade

This simulation includes meshing, fluid domain, boundary conditions inlet, outlet, walls, etc, that have the characteristics above mentioned.

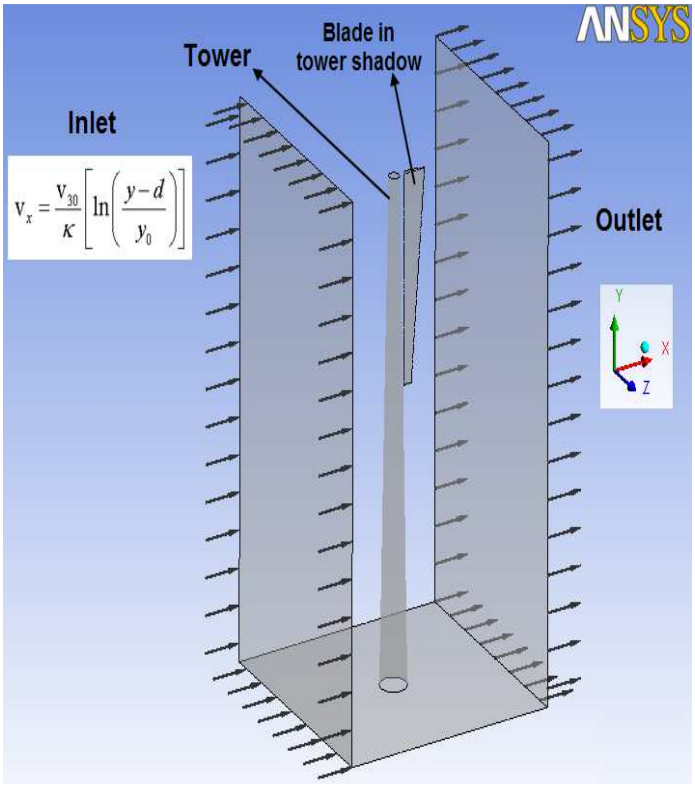

Figure 58. CFD simulation of the fluid channel with the wind turbine tower and blade in the channel. The blade is located in the tower shadow.

The Inlet specifies the magnitude and direction of the speed v_{air} that the fluid has when entering the channel. The direction is taken to be normal to the selected boundary surface. The Outlet sets the magnitude of the relative static pressure of the fluid, which is assumed to be 0 [Pa]. The Walls set a sliding surface of the fluid.

When defining the fluid domain parameters it was taken into account the high value of the Reynolds number, which is a clear indication that the fluid flow is characterized as turbulent.

Turbulence is a 3-D random unstable movement of the fluid, which is a characteristic for low-viscosity fluids. Multiple variables depend on the turbulence such as heat transfer, moments, pressure losses, aerodynamic forces, etc.

In general, turbulence is described by the Navier-Stokes set of equations, but in most cases it is not appropriate to solve fluid turbulence problems that account for turbulence by applying directly a given numerical method. This is due to the fact that the calculations are too complex and involve significant time and computational resources. Therefore, some

averaging procedures are applied to the Navier-Stokes equations, which filter the respective turbulence parts. Thus, a continuous variation of the fluid pressure and speed could be achieved. The process of averaging leads to the emergence of new unknowns in the equations. These unknowns are to be satisfied by well-known developed turbulent models such as k-Epsilon[2], Shear-stress transport[3] and others.

The efficiency and accuracy of the fluid simulation substantially depend on the selection of a suitable turbulent model which can provide for the necessary framework for solving the model. The present problem is analysed through simulations and comparison studies with the two turbulence models mentioned above. It was found that the Shear-stress transport model is suitable when the angle β increases over 10°, while the lower values of angle allow for both models to be used. The successful completion of CFD simulation provides opportunities for reporting numerous results at any point of the channel. Figure 59 presents simulation results from the simulation shown in Figure 57.

[2] ***The K-epsilon model*** *is one of the most common turbulence models, although it just doesn't perform well in cases of large adverse pressure gradients. It is a two equation model, that means, it includes two extra transport equations to represent the turbulent properties of the flow. This allows a two equation model to account for history effects like convection and diffusion of turbulent energy.*

[3] ***The shear stress transport (SST)*** *formulation combines the best of two worlds. The use of a k-ω formulation in the inner parts of the boundary layer makes the model directly usable all the way down to the wall through the viscous sub-layer, hence the SST k-ω model can be used as a Low-Re turbulence model without any extra damping functions. The SST formulation also switches to a k-ε behaviour in the free-stream and thereby avoids the common k-ω problem that the model is too sensitive to the inlet free-stream turbulence properties. Authors who use the SST k-ω model often merit it for its good behaviour in adverse pressure gradients and separating flow.*

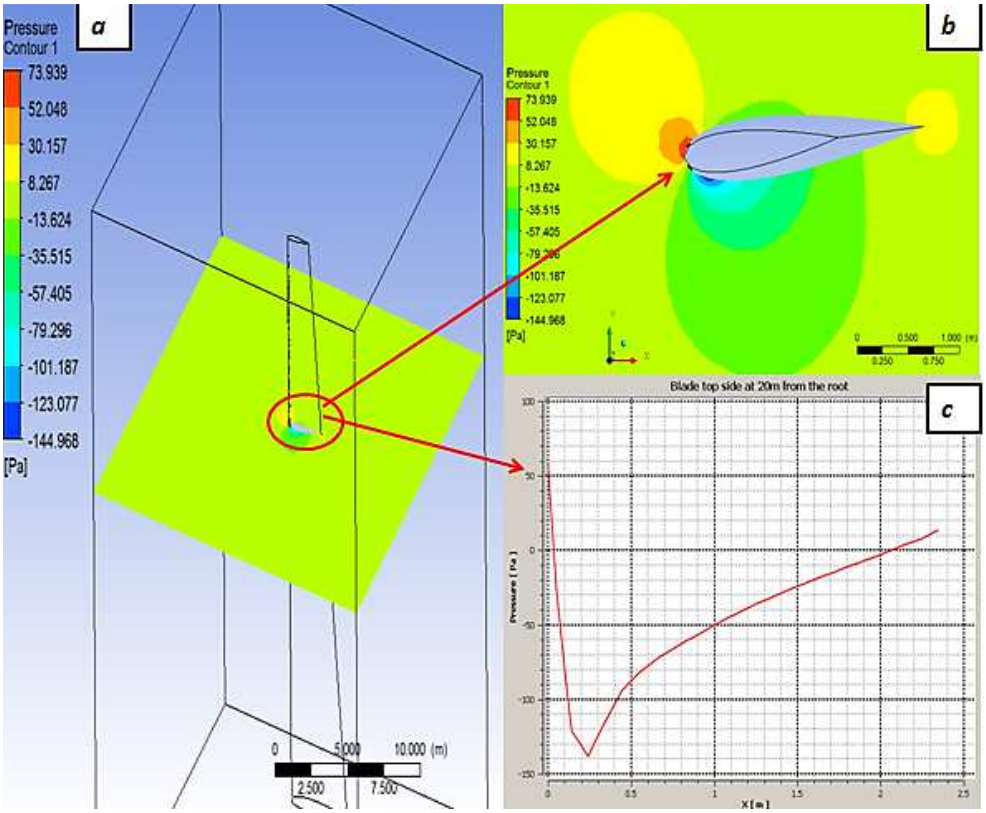

Figure 59. Fluid pressure distribution. a – in plane 20meters above the blade foundation; b – zoomed view of the section; c – graph of the pressure distribution

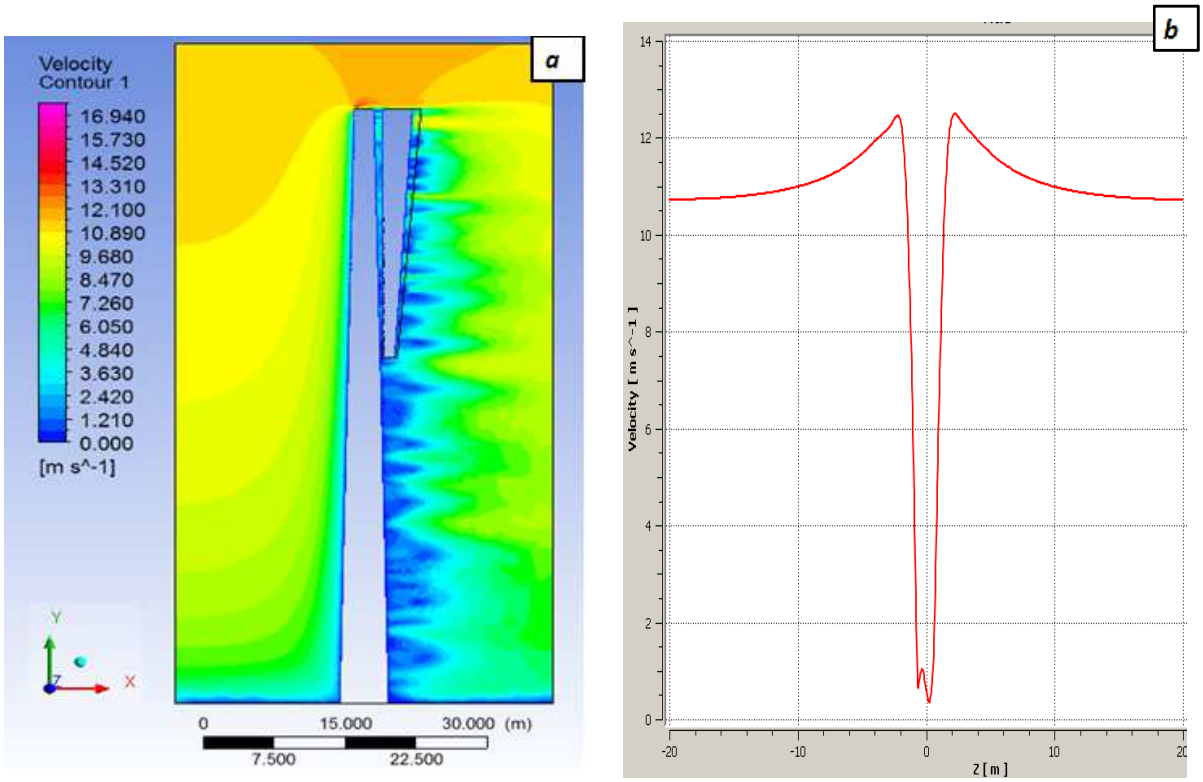

Figure 60. Fluid velocity distribution for the simulation in the previous figure a – XY cross-section through the plane of channel symmetry; b –XZ cross-section at y=42meters above the tower foundation, at x=2m from the tower centre.

A wind turbine with three blades suffers an undesirable effect known as the 3*p* effect. The 3*p* fluctuations are due to two effects known as wind shear and tower shadow. Wind shear refers to the variation of wind with height [Equation 23] while tower shadow is used to describe the redirection in wind due to the obstruction presented by the tower. These two effects are an inherent characteristic of any wind turbine and will result in periodic fluctuations in output power. Hence, the tower shadow affects the turbine dynamics, give power fluctuations and increases noise generation.

The CFD simulation results for the pressure variation on the surface of the submerged body were used as loading conditions for subsequent mechanical simulation of the body response. Briefly, the loading on each blade, nacelle and tower is determined through parallel fluid simulations, for a given moment of time, and then the results are used to generate the loading on the meshed model 3, Figure 61.

The issue of **model meshing** is crucial for the proper analysis of the problem. This is due on one hand to the fact that a good model approximation of the real object is achieved when the parameters of the virtual and real space are in coherence. On the other hand, the appropriate and well-defined mesh of the model could provide results that outline a detailed picture of the stress and strain state of the system, which is a difficult to achieve task for any analytical solution.

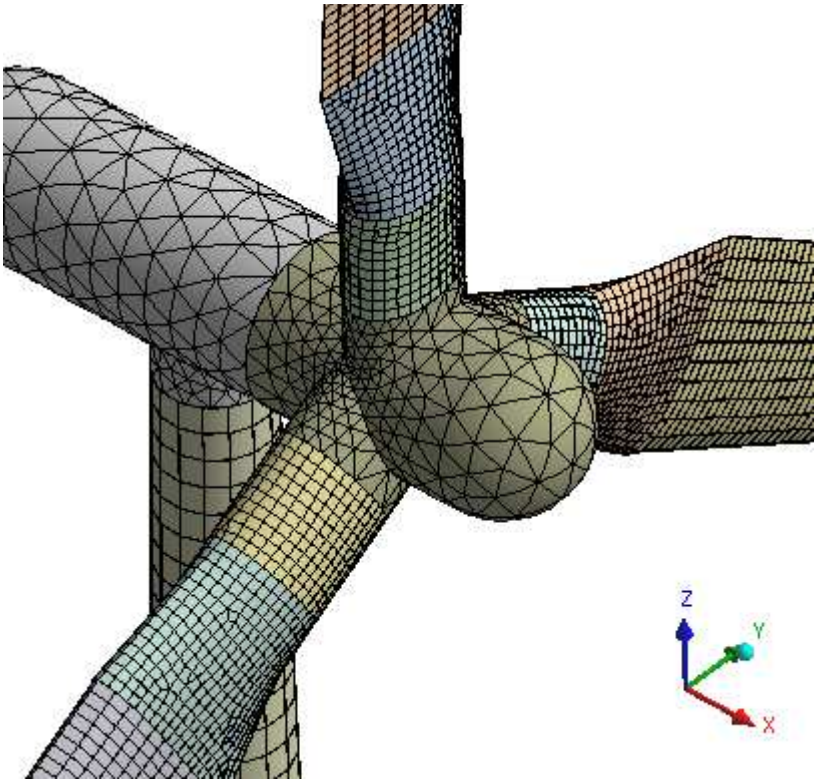

Figure 61. A fragment of the model 3 finite element mesh.

The model mesh consists mainly of the following elements:10 -Node Quadratic Tetrahedron, 20 -Node Quadratic Hexahedron and 20 -Node Quadratic Wedge. Contacts are meshed with Quadratic Quadrilateral (or Triangular) Contact and Target elements.

- **10-Node Quadratic Tetrahedron**. A finite element defined by 10 nodes with respective x y z translational degrees of freedom at each node. This element is assumed as suitable for this problem because of its ability to discretize the complex geometry.

- **20 -Node Quadratic Hexahedron**, Figure 62. This finite element is similar to the 10-Node Quadratic Tetrahedron. In addition, it uses 20 nodes, quadratic behaviour for the displacement and is implemented in the areas of uneven distribution of stresses.

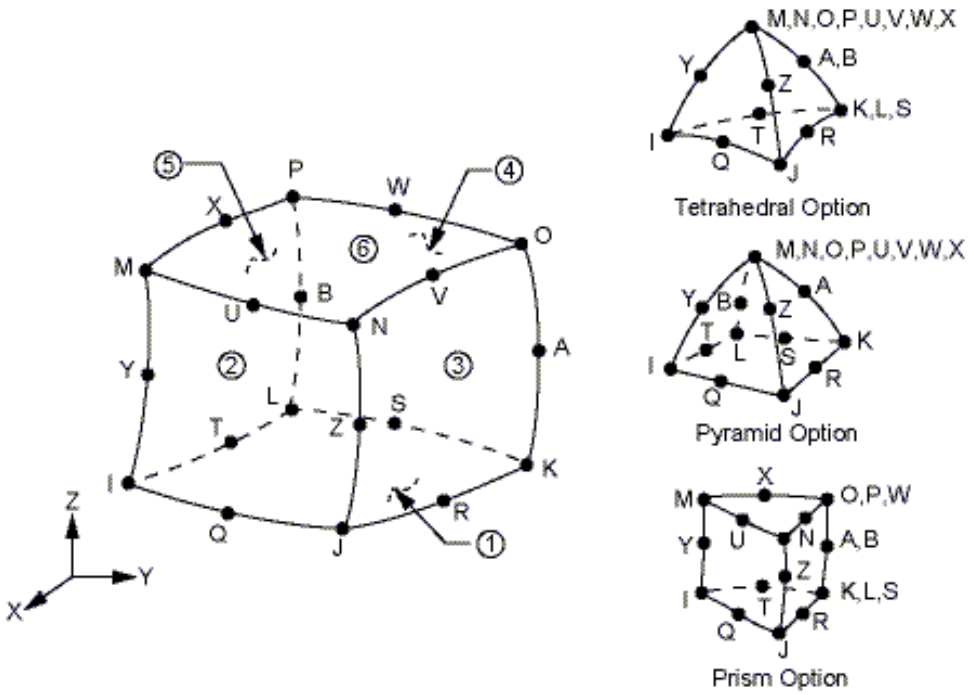

Figure 62. 20-Node Quadratic Hexahedron finite element

- **Quadratic Quadrilateral (or Triangular) contact elements**. Finite elements used to define the contacts between the wind turbine parts. These elements are characterized by 8 nodes, contact type surface-to-surface and perceive the parameters of the corresponding 3-D element to which they are attached.

During the step of meshing, the finite element mesh quality was examined in details in a manner similar to the control applied in the fluid simulations. Upon completion of this step, the fluid simulations loads are taken and applied.

In this way, it is possible to consider the response of the entire system for a given moment of time, e.g. when a sharp change of the wind occurs. When the wind turbine is to be controlled then it is mandatory to be able to react promptly to wind changes. However, the problems with large computational resources and time leads to the idea of applying concentrated equivalent loads based on the CFD results

7.2.4. Applying loads

Moreover, after the completion of a CFD simulation, for a single blade for example, there are obtained values of F_{Thrust} and F_{Torque}, as shown in Figure 63. In this case, the chord of the profile lies on the C1-C 2 axis. The moment of inertia about the chord is set in

[Equation 16] as J (x). Under the assumption of the equation, J (x) is determined with respect to the centroid of the profile to which a normal load on the axis n1-n2 is applied.

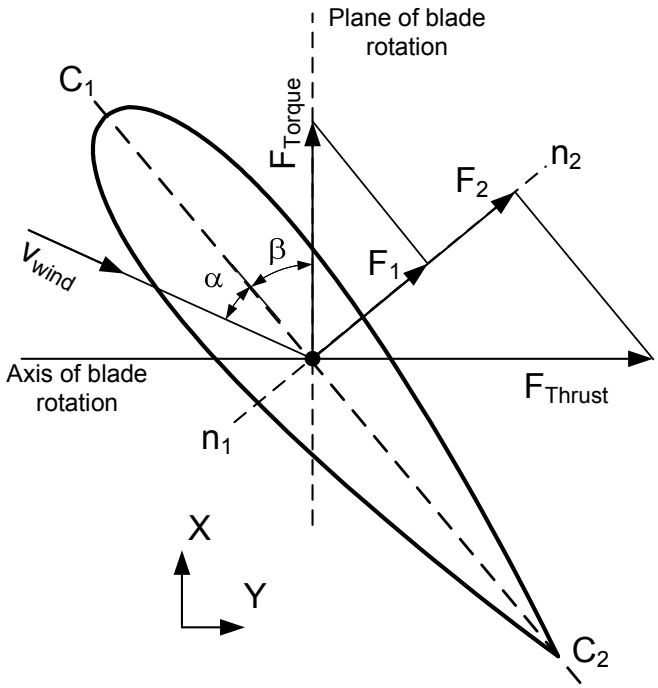

Figure 63. Blade loading.

In order to obtain normal load, F_{Thrust} and F_{Torque} are projected as F_2 and F_1, and model 1 and model 2 blade is loaded with the following:

$$F_{Blade}(t)\,\delta\left(x-\frac{L_B}{2}\right)=F_1+F_2 \quad \text{[Equation 23]}$$

For example, the resultant forces are applied to model 2, Figure 64. The main element in mesh is BEAM188 beam with quadratic behaviour for the displacement. It is suitable for analysing medium-thick and thick beam structures. It is based on the theory of Timoshenko[4] and features two nodes, each with six degrees of freedom. The tower and the blades are meshed with this element. It is necessary to load a certain cross-section with which the element would be engaged to carry out the study.

[4] ***Timoshenko model*** *takes into account shear deformation and rotational inertia effects, making it suitable for describing the behaviour of short beams, sandwich composite beams or beams subject to high-frequency excitation when the wavelength approaches the thickness of the beam.*

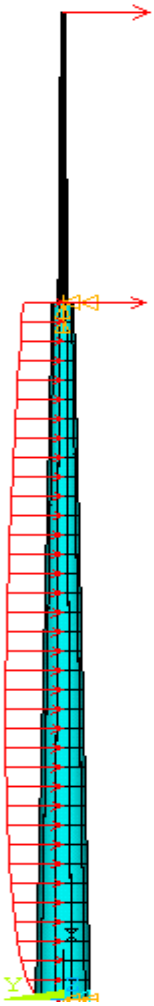

Figure 64. ANSYS model with applied loading

Attention should be paid in model 2 to the construction of the blade sections. While the tower allows for use of a simple tubular profile that is available as a ready-made element in the ANSYS library, the blades have to be generated in a specific way. Ten sections are selected from the SolidWorks 3-D geometry at equal intervals along the height of the blade Figure 65 .

Sections, Figure 65a are loaded sequentially into the library of the product, and after that starts the meshing of the blade as a beam structure Figure 65-b.

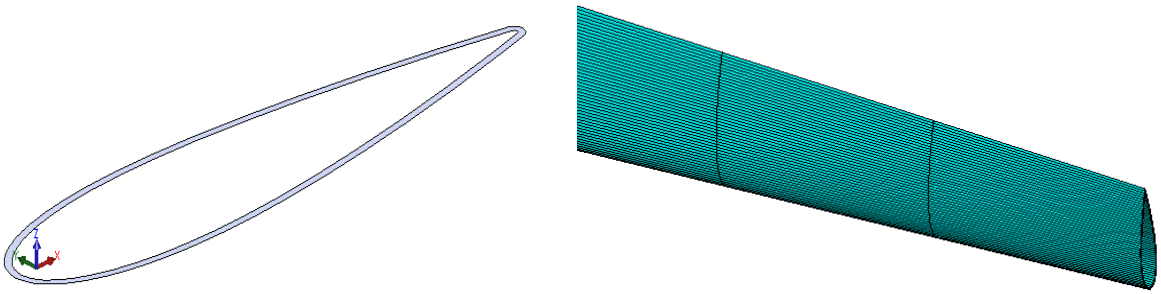

(a) (b)

Figure 65. Generating the blade geometry a) blade section; b) blade mesh

After the model 2 blade was loaded with the force from equation 24, the rest of the blades were loaded according to the Rotor Blade Theory assumption [15]. According to this assumption the rotor disk force is applied to the top of the tower as:

$$F_T(t)\delta(x-L_T)$$ [Equation 24]

The figures below depict the dynamic response of the tower and the blades as part of the system. The response is obtained by simulations with model 1 and model 3 both loaded with charged with $F_{Blade}(t)$ and $F_T(t)$, wind speed $v_{wind}=11\text{m/s}$ and blade pitch angle $\beta=10^{\circ}$.

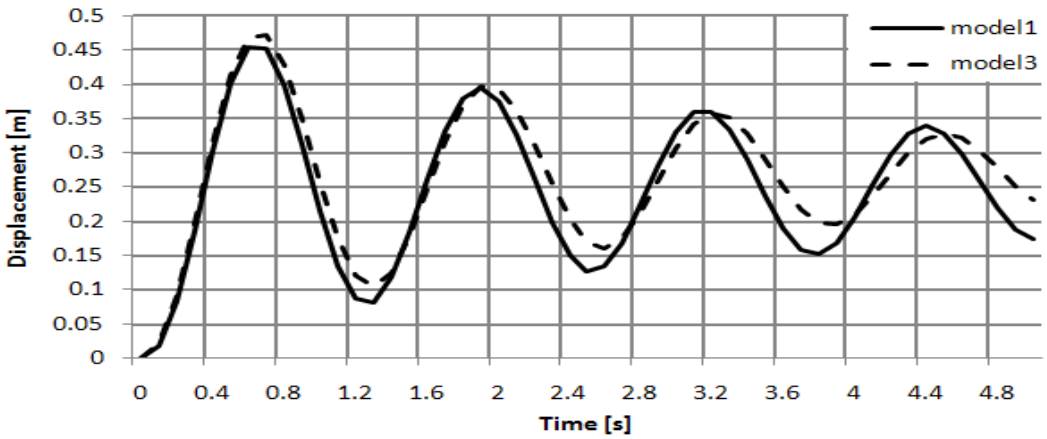

Figure 66. Displacement of the tower tip

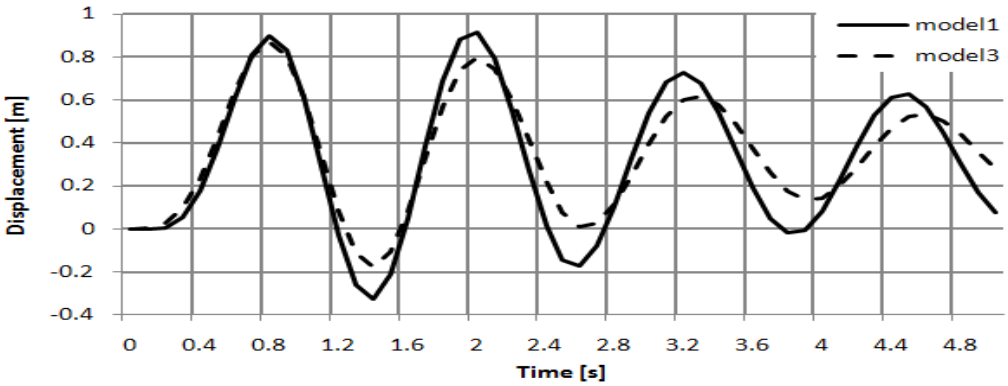

Figure 67. Displacement of the blade tip

7.2.5. Blades improvement

When choosing the design configuration of a wind turbine, including any further improvements, such as the type and size of the turbine, number and location, operation and maintenance strategies, etc., the economic numbers of profit from the turbine have to be considered. Usually, the following three general elements are included: (1) Capital cost, (2) operating and maintenance costs, and (3) energy output.

The recent development of cost models based on many wind turbines with three-bladed, pitch-controlled, variable-speed rotors [21] permits estimates of component cost contributions in more detail now than previously possible.

For example, Table 3 is an extended list of items to be considered when estimating the cost of a wind power production. In this example, the station has a rated capacity of approximately 51 MW and is composed of 34 mature-design turbines rated at 1.5 MW each.

Table 3. Estimate of cost contribution.

Rotor Assemblies		**16.9 %**
Blades	10.8 %	
Hub	3.1 %	
Pitch Mechanism & Bearings	2.7 %	
Spinner	0.3 %	
Nacelles and Power Trains		**46.4 % Turbine: 63.3 %**
Gearbox	10.8 %	
Variable-Speed Electronics	8.4 %	
Generator	7.0 %	
Main Structure	6.6 %	
Electrical Connections	4.3 %	
Control, Safety, & Condition Monitoring	2.5 %	
Low-Speed Shaft	1.5 %	
Nacelle Cover	1.5 %	
Yaw Drive and Bearing	1.4 %	
Hydraulic & Cooling Systems	1.3 %	
Bearings	0.9 %	
Mechanical Brakes, High-Speed Shaft, *etc*	0.2 %	
Towers		**10.5 %**
Balance of Station		**26.2 %**
Electrical Interface & Connections	8.7 %	
Roads, Civil Work, & Staging	5.6 %	
Transportation	3.6 %	
Foundations	3.3 %	
Assembly & Installation	2.7 %	
Permits, Engineering, & Site Assessment	2.3 %	
Initial Capital Cost of Wind Power Station		**100.0 %**

Taking a closer look it appears that the rotor assemblies contribute almost 17% to the total capital cost while the blades alone contribute to almost 11% of the cost. So it appears that the blades are not only the major "wind capturer" but also play a significant role from economic standpoint.

The current study could perform analyses of the various HAWT components but in view of the abovementioned statements, attention is paid towards the blade airfoil improvement. The topic is extremely large and that's why will be summarized with some

of the results obtained when selecting the airfoil NACA643218 as a modernizing option instead of the default design with NACA0021.

The **NACA-0021** airfoil is one of the NACA four-digit wing section series. It is a 21% thick, symmetrical airfoil with the point of maximum thickness located at x/c = 0.30, where x is the axial coordinate measured from the airfoil's nose and c is the chord length.

Advantages:

- good stall characteristics;
- roughness has little effect;

Disadvantages:

- low max lift coefficient;
- relatively high drag;

The **NACA-643218** airfoil is one of the NACA six-digit wing section series. The 6-series was derived using an improved theoretical method that, like the 1-Series, relied on specifying the desired pressure distribution and employed advanced mathematics to derive the required geometrical shape. The goal of this approach was to design airfoils that maximized the region over which the airflow remains laminar. In so doing, the drag over a small range of lift coefficients can be substantially reduced.

Figure 68 shows the NACA-0021 airfoil vs. the NACA-643218. Obviously the six-digit airfoil is much thinner which allows for material economies and reduction in weight. Evaluation confirmed that the NACA-643218 airfoil cross-section is with 19.55% less than the cross-sectional area of the NACA-0021.

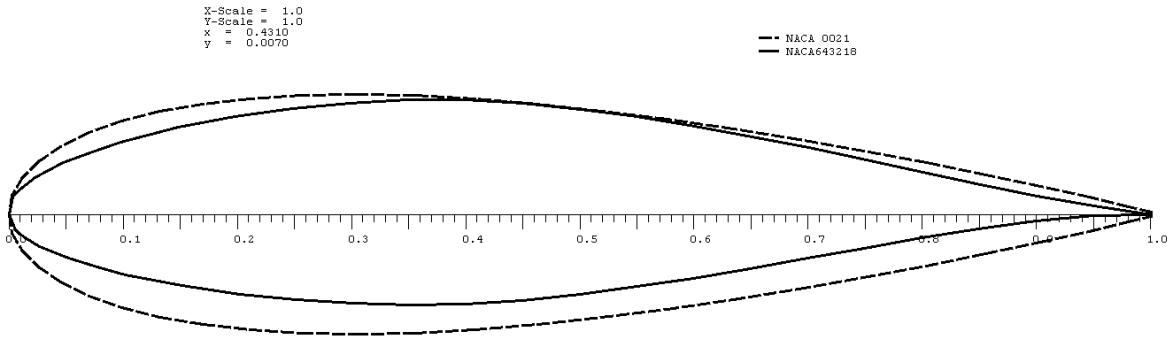

Figure 68. NACA0021 vs. NACA643218

Further the two airfoils are compared when used for constructing the blades of the studied HAWT.

7.2.6. Results

As is known differential pressure is what creates lift. The air flowing under the blade is of greater pressure than that flowing over the top. The high pressure air beneath the blade is trying to find a way to get to the top in order to equalize the pressure. It cannot flow inward toward the rotor so it flows outward toward the tip. At the blade tip, the high pressure air under the wing will actually whip around the tip in order to reach the low pressure air on top. This phenomenon is what creates the vortices known as wake turbulence. These vortices wouldn't be formed if there weren't some spanwise flow outward beneath the wing toward the tip.

An assumption associated with the development of the BEM theory is that spanwise flow is negligible, and therefore airfoil data taken from two-dimensional section tests are acceptable.

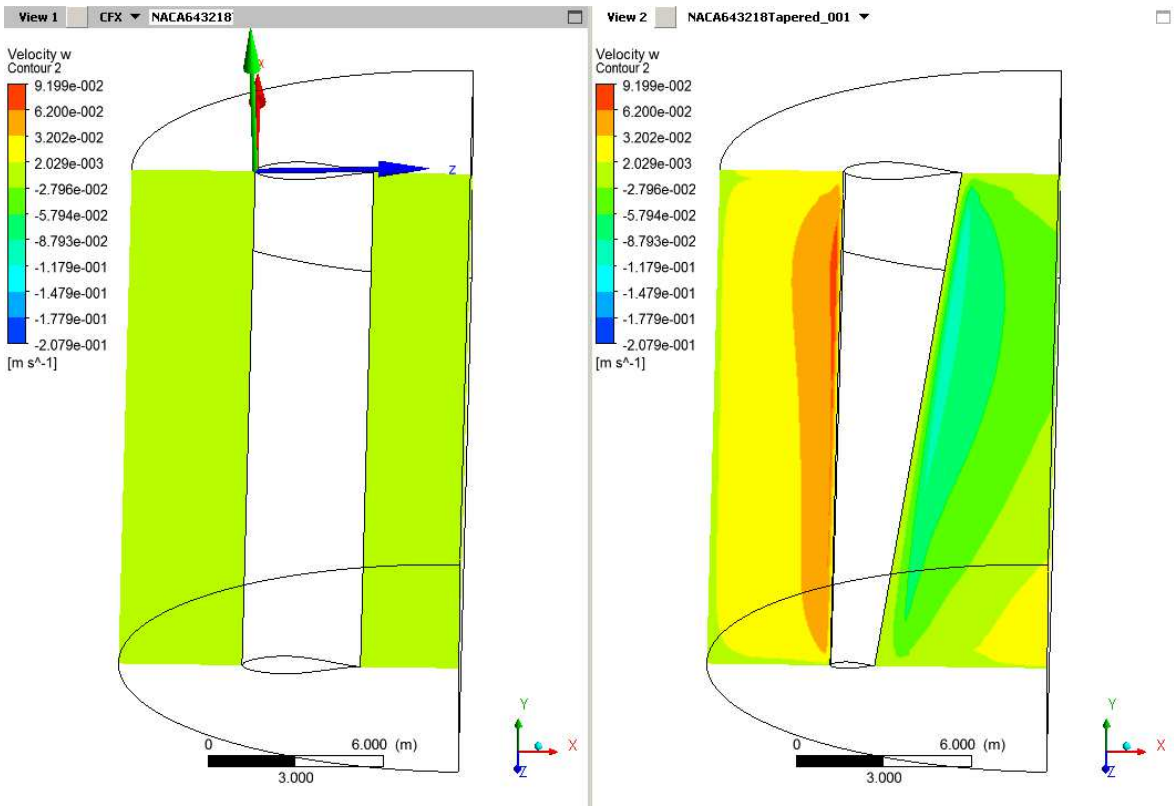

Figure 69. NACA-643218 non-tapered vs. tapered, wind span wise velocity, Vz

Therefore, when a blade is not perpendicular to the axis of rotation (e.g., when the blade has a coning angle, tapered) the wind has a component that is directed along the span of the blade, as confirmed by Figure 69. However, BEM theory does not predict any

induced flows along the blades and this component is usually neglected by this theory and two-dimensional flow is assumed, adding some error to the airfoil data.

The next figures and tables present more details in the comparison analysis of the discussed blade airfoils.

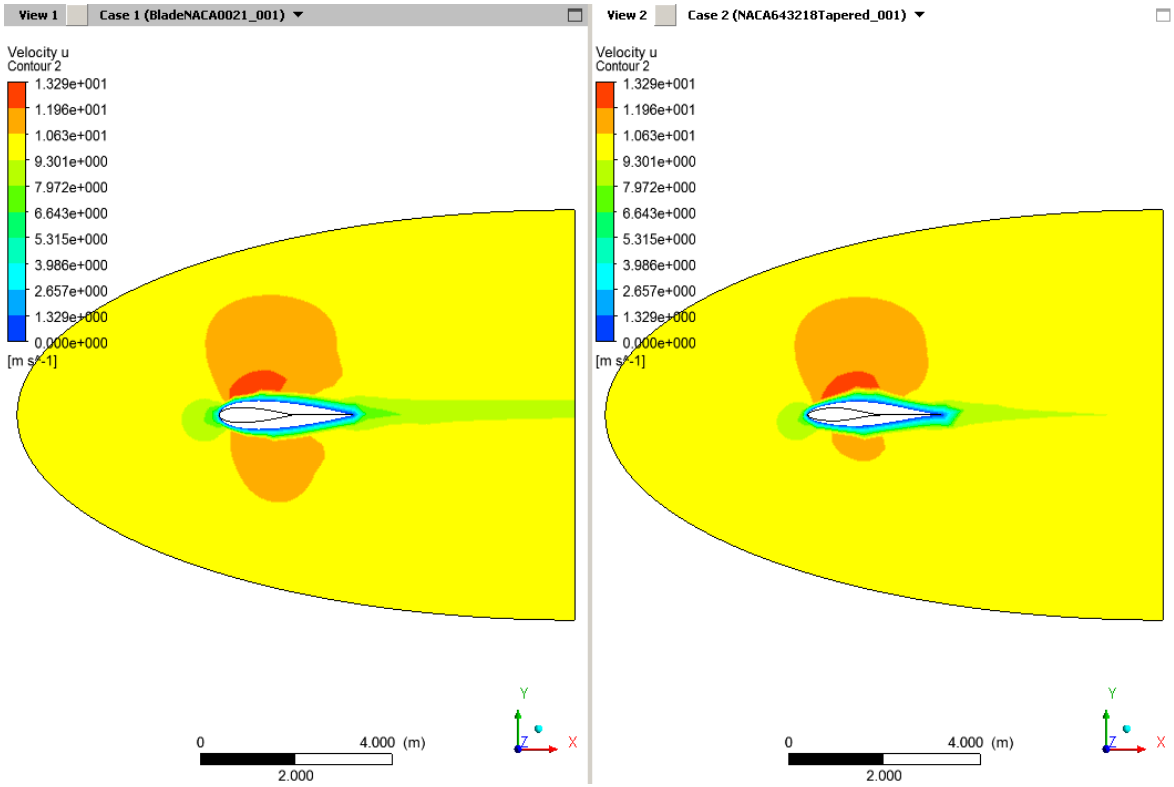

Figure 70. NACA-0021 tapered vs NACA-643218 tapered, wind velocity, Vx, α=2deg

As mentioned before, the NACA643218 airfoil is one of the NACA six-digit airfoil series with the goal of maximizing the region over which the airflow remains laminar. Figure 70 shows a comparison between the 4- and the 6-digit airfoils. It is obvious that the laminar region over the NACA643218 is of higher proportion than the laminar region over the NACA0021.

In the next figure, it can be seen how the NACA643218 airfoil obtain a better relation Cl/Cd. The tangent to the curve from the Cl/Cd origin shows the best Cl/Cd ratio, and thus the best glide angle you can get. The best NACA643218 Cl/Cd ratio is slightly greater than the NACA0021 ones.

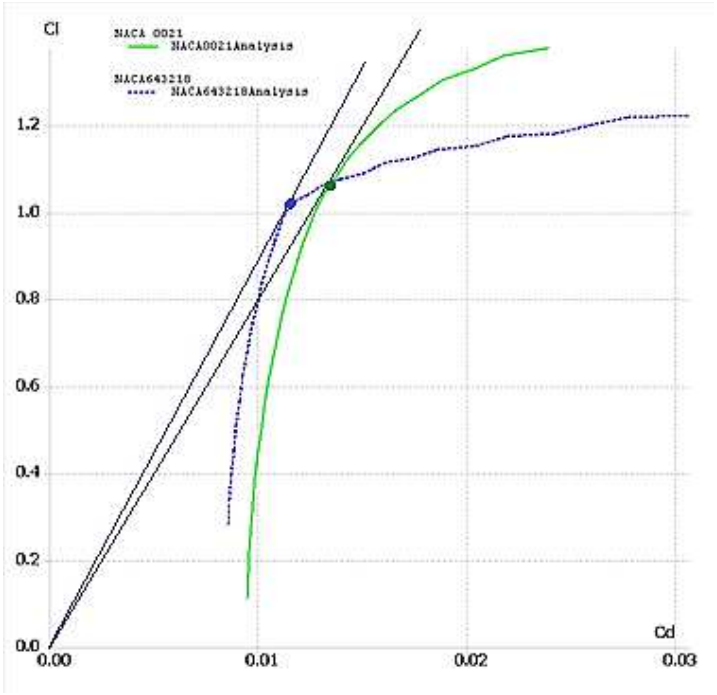

Figure 71. NACA-0021 and NACA-643218 lift coefficient vs drag coefficient

The figure below shows how lift resulting from the incident wind force increases as the angle of attack increases from 0 to a maximum of about 15 degrees at which point the smooth laminar flow of the air over the blade ceases and the air flow over the blade separates from the aerofoil and becomes turbulent. Above this point the lift force deteriorates rapidly while drag increases leading to a stall.

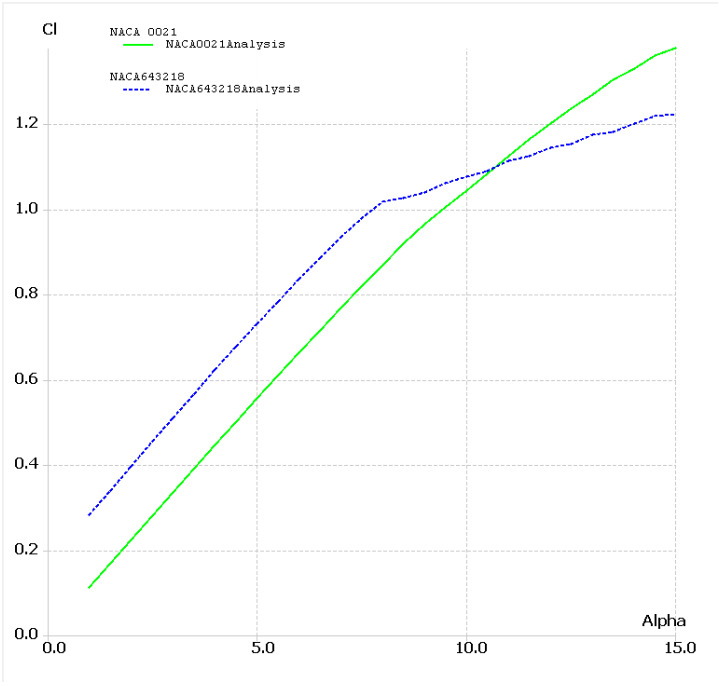

Figure 72. NACA0021 and NACA643218 lift coefficient vs angle of attack

From the next graph, the optimum angle of attack can be obtained. In this case, for a wind speed and a rotor angular velocity determined, NACA643218 is designed for an optimum angle of attack about 8º and NACA0021 airfoil is designed for an optimum angle of attack of 10º.

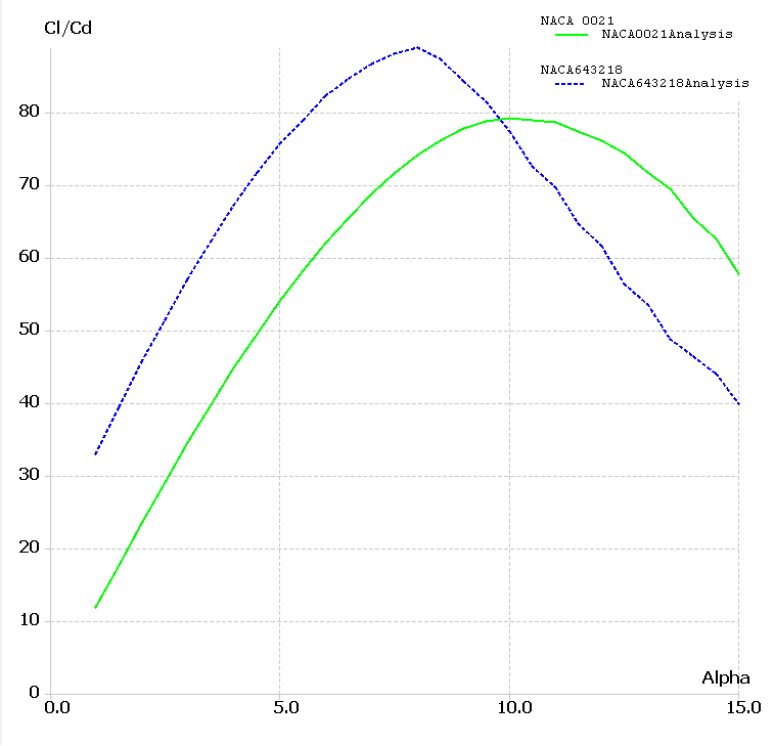

Figure 73. NACA-0021 and NACA-643218 Cl/Cd vs angle of attack.

In reference to figures 72 and 73, It is computed that for small α, in the range of 1-10deg, the 6-digit airfoil lift coefficient is with approx. 30% higher and similar assertion is valid for the Cl/Cd ratio vs Alpha (the angle of attack, α).

Wind turbines operate in a wide range of TSRs. Usually, the safe operation is within a range of wind speeds, starting from a cut-in wind speed of 5-6m/s and going up to 30-32m/s cut-out wind speed.

Figure 74 and **¡Error! No se encuentra el origen de la referencia.** show some of the obtained values for a range of 1-10 tip-speed ratio (TSR) for 3-bladed rotors.

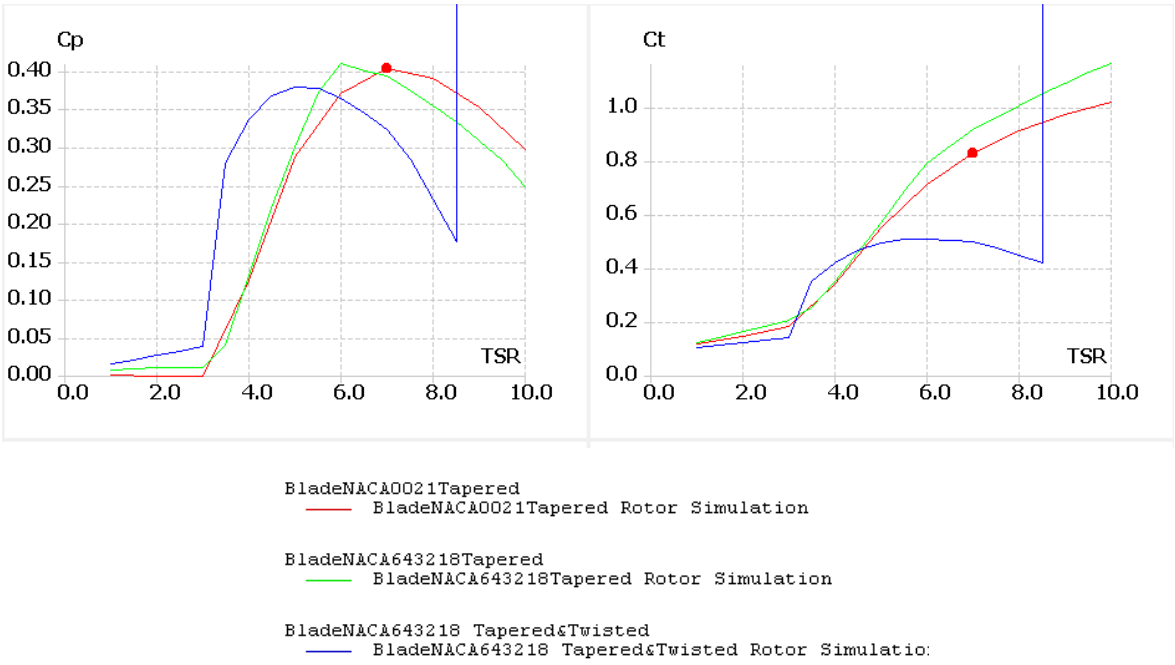

Figure 74. Power and thrust coefficients comparison of three types of 3-bladed HAWT rotors, NACA-0021Tapered, NACA-643218 Tapered and NACA643218 Tapered & Twisted.

Table 4. Comparison of Power coefficient Cp of the three rotors for a range of TSR.

	POWER COEFFICIENT C_P		
TSR	**NACA0021 Tapered**	**NACA643218 Tapered**	**NACA643218 Tapered &Twisted**
1	0.001617579	0.007399329	0.01482734
2	0	0.01048688	0.02669607
3	0	0.01098828	0.03870593
4	0.1243573	0.1317067	0.3361276
5	0.2863472	0.2998748	0.3786016
6	0.3709443	0.4085679	0.3636798
7	0.4020656	0.3938199	0.3233229
8	0.3893852	0.3540102	0.2315012
9	0.3516867	0.3086178	
10	0.2970206	0.2474009	

The tapered & twisted blade possesses a much higher lift for TSR below 5. However, it is an exemplary design of blade twist and it is a subject of further modifications.

As to the power coefficient, Cp, the two rotors with blade airfoils NACA0021 Tapered and NACA643218 Tapered, show some proximity in Cp values for TSR up to 5deg. Variations are 3% to 5%. The max Cp for NACA0021 is 0.40206 and for NACA643218 it

is 0.40857, which is 1.5% higher. The max Cp is obtained for different TSRs, respectively 6 for NACA643218 and 7 for NACA0021.

Besides, in the following Figure, it can be seen the variation of the angle of attack along the blade length in the NACA0021 airfoil for different values of TSR:

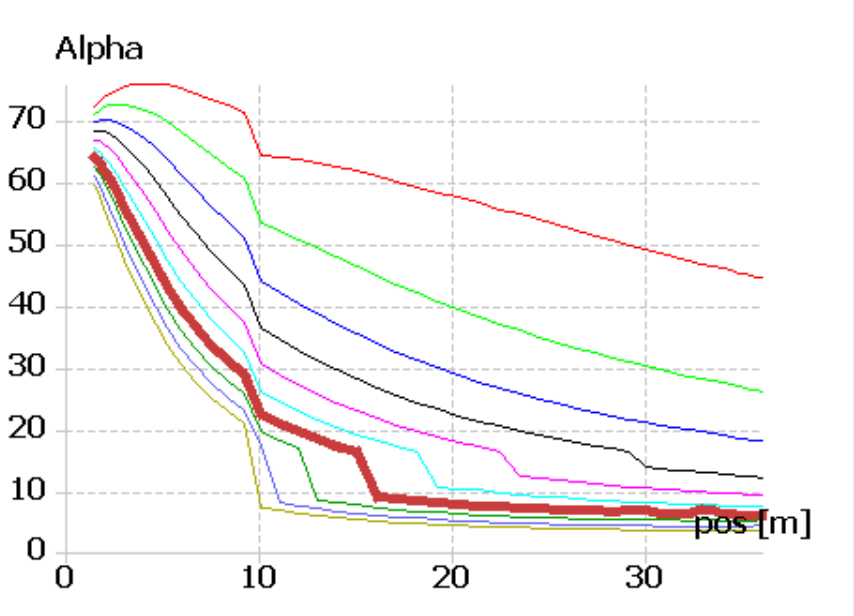

Figure 75. NACA0021 angle of attack vs. blade section position from the root of the blade.

The most highlight line represents the variation of the angle of attack when the blade is in the red point situation (TSR=7) shows in Figure 74. In addition, when the wind turbine works with a greater value of TSR than this value, the power efficiency decreases because the power coefficient becomes lower as a consequence of the starting stall.

The tangential velocity 'V' of any blade section at a distance 'r' from the centre of rotation (the root of the blade) is given by $V = r\,\Omega\,(1+a')$ where Ω is the angular velocity of rotation in radians and a' is an correction factor. Thus, for a given wind speed the apparent wind will be different at the root of the blade from the apparent wind at the tip of the blade because the rotational relative wind speed is different.

For a given wind speed, angular velocity and blade pitch (no twisted blades like this airfoil example NACA0021 tapered in Figure 75), the angle of attack at the blade root is higher because the tangential speed of the airfoil is lower at the blade root.

Hence, to retain the optimum angle of attack along the blade length, for a determinate value of TSR, it has been shown that is not enough to have a tapered blade but also a twist

must be done as it approaches the blade root. The necessary pitch angle or twist grade through the blade is determinate by the optimum designed angle of attack of the Apparent wind, i.e., is necessary to twist the blade to maintain a given angle of attack along the blade to which the lift coefficient is maximal.

The Apparent wind (W) is de vector sum of the Actual wind (U) and the Relative wind (V) caused by the rotation of the blade through the air.

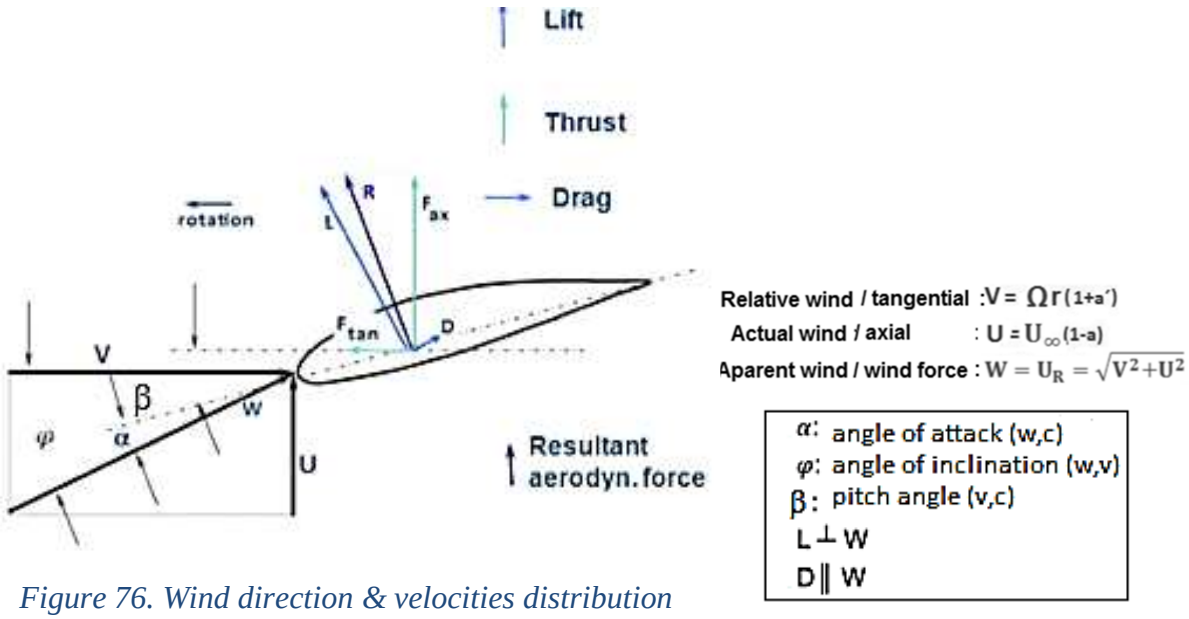

Figure 76. Wind direction & velocities distribution on a blade section.

The figure below shows the tangential velocity and pitch angle increase along the blade.

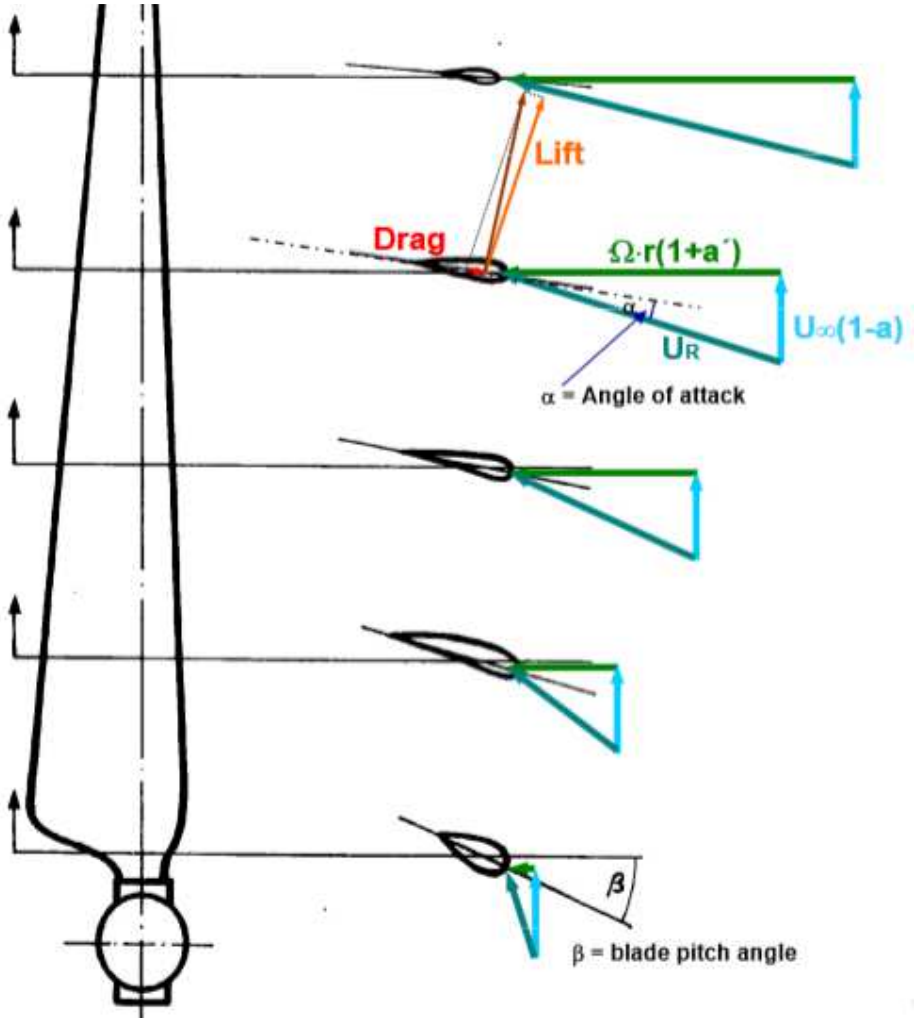

Figure 77. Increased tangential velocity of sections of the blade in a twisted blade to maintain the optimum angle of attack

.

As the wind speed changes however, the twist will no longer be optimum. To retain the optimum angle of attack as wind speed increases a fixed pitch blade (stall control rotors) must increase its rotational speed accordingly, otherwise, for fixed speed rotors, variable pitch blades(pitch control or active stall control rotors) must be used. These different types of control have been mentioned in section 3.2.4.

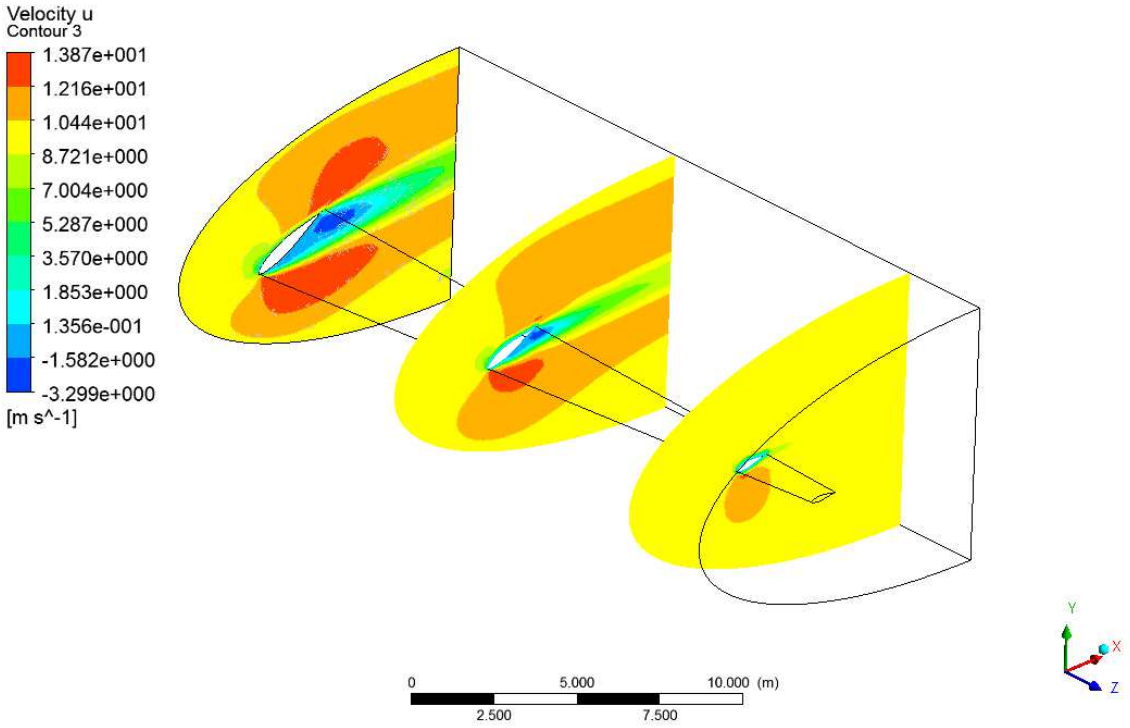

Figure 78. Wind velocity Vx, in sections of the NACA643218 Tapered & Twisted blade.

When the NACA643218 blade is tapered and twisted, the analysis becomes even more complicated. Figure 78, shows such a blade, for α=2deg, and several planes with wind velocity V_x contours. Near the blade root, significant eddy regions are formed. In this figure is not possible to appreciate the tangential velocity increase along the blade because the blade rotation has not been simulated.

Table 5. Comparison of Cl for NACA0021 and NACA643218, CFD vs BEM.

LIFT COEFFICIENT C_L

NACA0021		Error %	**NACA643218**		Error %
CFD	BEM		CFD	BEM	
0.21626	0.224932	4.01	0.38371	0.395664	3.11
β=2deg, Re≈9.1×10^6, M≈0.03					

Figure 71, Figure 72, Figure 73 and **¡Error! No se encuentra el origen de la referencia.** and Table 5 show the two-dimensional lift, drag and power coefficients comparison between NACA-0021 and NACA-643215 rotor blades.

Table 5 confirms the validity of the performed simulations by comparing the CFD and BEM results of the lift coefficient for both NACA-0021 and NACA-643215 airfoils. The

obtained error is within acceptable limits, but for more precise investigations it is possible to improve the mesh of finite elements for the CFD simulations.

It could be noted that in order to achieve the maximum lift and efficiency for some long blades, not only the chord length, thickness and twisted angle change, but also the shape of airfoil varies along the blade. Manufacturing difficulty, however, needs to be taken into account as well.

8. CONCLUSIONS

For reasons of efficiency, control, noise and aesthetics the modern wind turbine market is dominated by the horizontally mounted three blade design, with the use of yaw and pitch, for its ability to survive and operate under varying wind conditions.

In this study, developed are models, for analysis with distributed loading of a HAWT under wind which first reaches the tower and then the blades (downwind wind turbine).

The created finite element models account for the tower, the nacelle and the blades, assuming that the tower and blades are systems with distributed parameters and the nacelle is concentrated mass.

Developed is a software implementation of the model and the results are compared the results from 3 -D model simulations developed in ANSYS.

The models can be used for identification and optimization of the parameters of the system. It is also possible that they be used for modal analysis of the system and for the generation of reduced models for the first few natural mode shapes and frequencies. Similar models can be actively used in the synthesis of control systems of HAWT, as well as in the study of the HAWT fatigue behaviour.

This project has provided results of investigation into the capabilities and accuracy of various computational tools like the finite element method (FEM), the blade element method (BEM), the Newmark method, computational fluid dynamics (CFD) and others for simulating and analysing the response of the HAWT both in its default design configuration and in the improved design configuration.

Assumptions that spanwise flow is negligible and therefore airfoil data taken from two-dimensional section tests are acceptable have been reaffirmed.

Rotors with blades airfoils of NACA-0021 and NACA-643218 have been compared. The 6-digit series has been confirmed to maximize the region over which the airflow is laminar. As to the power coefficient, both airfoils show some minor variations but the most important one is that the 6-digit series airfoil provides the max. Cp at a lower TSR.

HAWTs usually operate in the post-stall regime, so accurate predications in this area are important. While this is a dynamic environment rather than a static one, the static CFD calculations performed are a prerequisite to accurate dynamic calculations.

It has been shown that the default turbulence model in most CFD codes, the k-e model, is not sufficient for accurate aerodynamic predictions so the shear stress transport (SST) model was applied but an extensive investigation is required to determine the best transition and turbulence models for wind turbine application.

The validity of the performed simulations has been confirmed by comparing the CFD and BEM results of the lift coefficient for two types of airfoils. However, for more precise investigations it is possible to improve the mesh of finite elements for the CFD simulations.

When the wind turbine is to be controlled then it is mandatory to be able to react promptly to wind changes. However, the problems with large computational resources and time leads to the idea of applying concentrated equivalent loads based on the CFD results. Therefore, it would be an interesting idea in future investigations to simulate the rotor rotation in order to observe the difference of the wind load applied in function of the position of the blade in the rotation plane.

9. REFERENCES

[1]. Independent Statics & Analysis Energy Information Administration http://www.eia.gov/

[2]. Pike Research´s report: Offshore Wind Power. 2011, Boston, United States.

[3]. Computational fluid dynamics of wind turbine blade at various angles of attack and low Reynolds number. S.Rajakumar. International Journal of Engineering Science and Technology. Vol.2. 2010, 6474-6484.

[4]. Wind turbines. Mechanical Engineering. Boston University.

[5]. Wind turbines control systems. Principes, modelling and gain scheduling design. Bianchi, F.D; Battista,H;Mantz, R.J 2007.

[6]. Wind turbines aerodynamics and wind characteristics. Joseba Ripa. Energy technology. Public University of Navarre.

[7]. Renewable energy: technology, economics, and environment" by Martin Kaltschmitt, Wolfgang Streicher, Andreas Wiese, (Springer, 2007, ISBN 3-540-70947-9, ISBN 978-3-540-70947-3), page 55.

[8]. Wind Power in Power Systems. Thomas Ackermann. John Wiley & Sons.2012

[9]. Hau, Erich, “Wind Turbines: Fundamentals, Technologies, Application, Economics”, Springer, 2000.

[10]. Fingersh, L., M. Hand, and A. Laxson, Wind Turbine Design Cost and Scaling Model, 2006

[11]. Matt Hein, Whitney Karpen, “Analysis of Wind Turbine Transverse Vibration”, Fluid Mechanics and Thermodynamics of Turbomachinery, 2005

[12]. D.A. Wright “Modern Control Design for Flexible Wind Turbines”, Technical report, National Renewable Energy Laboratory, NREL/TP-500-35816O, 2004

[13]. H. M. Negm, K. Y. Maalawi, “Structural Design Optimization of Wind Turbine Towers”, Computers and Structures, Elsevier, 2000.

[14]. C. Bottasso, A. Croce, B. Savini,W. Sirchi, L. Trainelli, AEROELASTIC MODELING AND CONTROL OF WIND TURBINE GENERATORS USING FINITE ELEMENT MULTIBODY PROCEDURES. MULTIBODY DYNAMICS 2005, ECCOMAS Thematic Conference.

[15]. T. Burton, D. Sharpe, N. Jenkins and E. A. Bossanyi, Wind Energy Handbook, John Wiley & Sons, Ltd, NY; 2001.

[16]. Shashikanth Suryanarayanan and Amit Dixit, On the Dynamics of the Pitch Control Loop in Horizontal-Axis Large Wind Turbines , 2005 American Control Conference June 8-10, 2005. Portland, OR, USA

[17]. S. S. Rao, The Finite Element Method in Engineering, 4th Edition, Elsevier Science, 2004, ISBN 0750678283

[18]. ANSYS, Theory reference, 2007

[19]. J. D. Anderson, Introduction to Flight, McGraw-Hill, ISBN 0-07-282569-3, 2004

[20]. T. R. Oke, Boundary Layer Climates, Methuen, 1987

[21]. Fingersh, L., M. Hand, and A. Laxson, Wind Turbine Design Cost and Scaling Model, NREL-TP-500-40566, Golden, Colorado, 2006